JPL PUBLICATION 81-40

Optical Deep Space Communication via Relay Satellite

Robert M. Gagliardi
Victor A. Vilnrotter
Samuel J. Dolinar, Jr.

August 15, 1981

National Aeronautics and
Space Administration

Jet Propulsion Laboratory
California Institute of Technology
Pasadena, California

TECHNICAL REPORT STANDARD TITLE PAGE

1. Report No. JPL Pub 81-40	2. Government Accession No.	3. Recipient's Catalog No.
4. Title and Subtitle Optical Deep Space Communication via Relay Satellite		5. Report Date 8-15-81 6. Performing Organization Code
7. Author(s) R. Gagliardi/V. Vilnrotter/S. Dolinar		8. Performing Organization Report No.
9. Performing Organization Name and Address JET PROPULSION LABORATORY California Institute of Technology 4800 Oak Grove Drive Pasadena, California 91103		10. Work Unit No. 11. Contract or Grant No. NAS 7-100 13. Type of Report and Period Covered JPL Pub
12. Sponsoring Agency Name and Address NATIONAL AERONAUTICS AND SPACE ADMINISTRATION Washington, D.C. 20546		14. Sponsoring Agency Code RD141 G-310-40-73-55-00

15. Supplementary Notes

16. Abstract

A study of the possible utilization of optical communications for a deep space link via an Earth-orbiting relay satellite is presented. The optical link is used primarily for high rate data transmission from a deep space vehicle to the relay, while RF links are envisioned for the relay to Earth link. This type of proposed hybrid system combines the advantages of optical frequencies for the free space channel to the relay with the advantages of RF links for atmospheric transmission. Auxiliary optical beacon and low rate RF links may be included for aiding pointing, tracking and timing operations.

A preliminary link analysis is presented for initial sizing of optical components and power levels, in terms of achievable data rates and feasible range distances. Modulation formats are restricted to pulsed laser operation, involving both coded and uncoded schemes. The advantage of an optical link over present RF deep space link capabilities is shown.

The problems of acquisition, pointing and tracking with narrow optical beams are presented and discussed in detail. Performance curves exhibiting degradation due to pointing errors, inaccurate beacon tracking and background clutter effects are shown. Mathematical models of beam trackers are derived, aiding in the design of such systems for minimizing beam pointing errors. A discussion of the expected orbital geometry between spacecraft and relay satellite, and its impact on beam pointing dynamics, is also included.

17. Key Words (Selected by Author(s))	18. Distribution Statement
Spacecraft Communications, Command, and Tracking Communications Optical Detection	Unclassified - Unlimited

19. Security Classif. (of this report)	20. Security Classif. (of this page)	21. No. of Pages	22. Price
Unclassified	Unclassified	67	

JPL PUBLICATION 81-40

Optical Deep Space Communication via Relay Satellite

Robert M. Gagliardi
Victor A. Vilnrotter
Samuel J. Dolinar, Jr.

August 15, 1981

National Aeronautics and
Space Administration

Jet Propulsion Laboratory
California Institute of Technology
Pasadena, California

The research described in this publication was carried out by the Jet Propulsion Laboratory, California Institute of Technology, under contract with the National Aeronautics and Space Administration.

CONTENTS

CONTENTS (Continued)

Figures

Figures (Continued)

ABSTRACT

A study of the possible utilization of optical communications for a deep space link via an Earth-orbiting relay satellite is presented. The optical link is used primarily for high rate data transmission from a deep space vehicle to the relay, while RF links are envisioned for the relay to Earth link. This type of hybrid system combines the advantages of optical frequencies for the free space channel to the relay with the advantages of RF links for atmospheric transmission. Auxiliary optical beacon and low rate RF links may be included for aiding pointing, tracking and timing operations.

A preliminary link analysis is presented for initial sizing of optical components and power levels in terms of achievable data rates at various distances. Modulation formats are restricted to pulsed laser operation, involving both coded and uncoded schemes. The advantage of an optical link over present RF deep space link capabilities is shown.

The problems of acquisition, pointing and tracking with narrow optical beams are presented and discussed in detail. Performance curves exhibiting degradation due to pointing errors and background clutter effects are shown. Mathematical models of beam trackers are derived, aiding in the design of such systems for minimizing beam pointing errors. A discussion of the expected orbital geometry between spacecraft and relay satellite, and its impact on beam pointing dynamics, is also included.

Since the modulation formats of the optical link to the relay and the RF link from the relay may be significantly different, an interface problem may arise in interconnecting the two links at the relay. This requires reformatting the detected optical signals to conform to the retransmitted RF link. The interface problem is discussed and several design alternatives are presented.

SECTION 1

THE OPTICAL DEEP SPACE RELAY SYSTEM

1.1 INTRODUCTION

In an earlier study (Ref. 1) the feasibility of an Earth-based deep space optical communication system was explored. Although the clear weather advantages of such a system were demonstrated, it was also pointed out that the deleterious effects of atmosphere, weather, and turbulence must be taken into account. These effects combine to introduce direct attenuation and possible outage times, and place restrictions on the minimal values of beamwidths and pointing accuracies.

A system that retains the advantages of the optical channel while avoiding weather effects is the optical relay system. Here a satellite relay, located outside the Earth's atmosphere, maintains an optical receiver for the reception of deep space transmissions. The free space link between the space vehicle and the proposed relay provides a distortionless environment for optical data transmission. The optical receiver operates in conjunction with an RF terrestrial link for data return to Earth. The optics is used for high rate data transmission and accurate pointing, while the RF serves primarily for link maintenance, back-up communications, and relay to Earth links. It is likely that any operational deep space optical link will evolve initially as some type of RF-optical hybrid system similar to that envisioned here. In this report some preliminary design considerations, performance capabilities, and apparent problem areas are presented for a hypothetical optical deep space relay system.

The relay system is diagrammed in Fig. 1-1. A planetary deep space vehicle transmits its data through an optical link to the relay. The latter is a satellite in geostationary orbit which contains the necessary optics for receiving and processing the transmitted field. The collected data is returned to Earth via an RF terrestrial link. An RF link from the Earth station to the spacecraft is also shown; it can be used for navigation, pointing, command, and auxiliary communications. An optical beacon is utilized from the relay to the spacecraft to improve the pointing of the optical data beam.

Figure 1-2 shows a block diagram of the basic spacecraft and relay subsystems. Spacecraft data is modulated onto the optical carrier for transmission to the relay as a narrow optical beam. The optical system aboard the relay photodetects the impinging beam and processes the data. The latter is relayed to Earth through modulation on a standard terrestrial RF link. The relay also transmits an optical beacon (CW or pulsed) to the spacecraft for spacecraft pointing. The beacon is tracked at the spacecraft and used to point the transmitting optics towards the relay.

1.2 THE OPTICAL DATA LINK

The optical transmitter aboard the spacecraft is assumed to consist of a laser with the appropriate modulation systems, and a circular diffraction-limited optical antenna of area A_t. If the spacecraft transmits an average

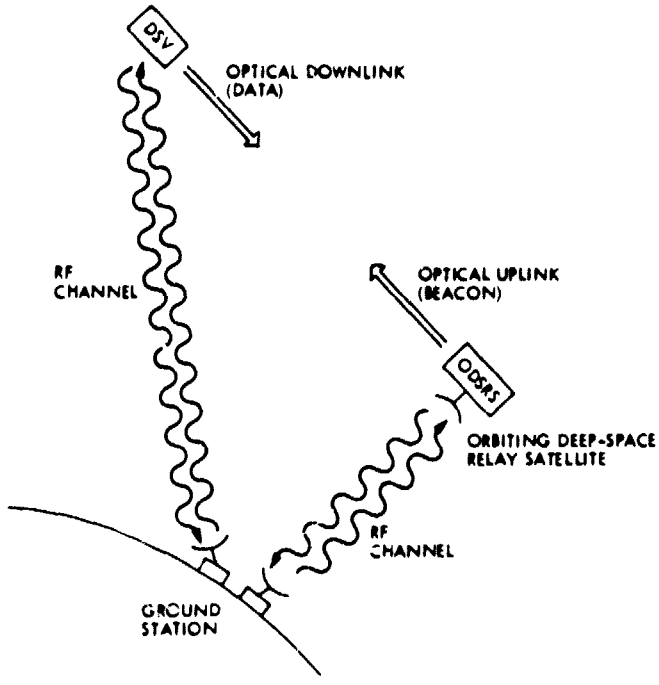

Figure 1-1. Optical Deep Space Relay Communication System

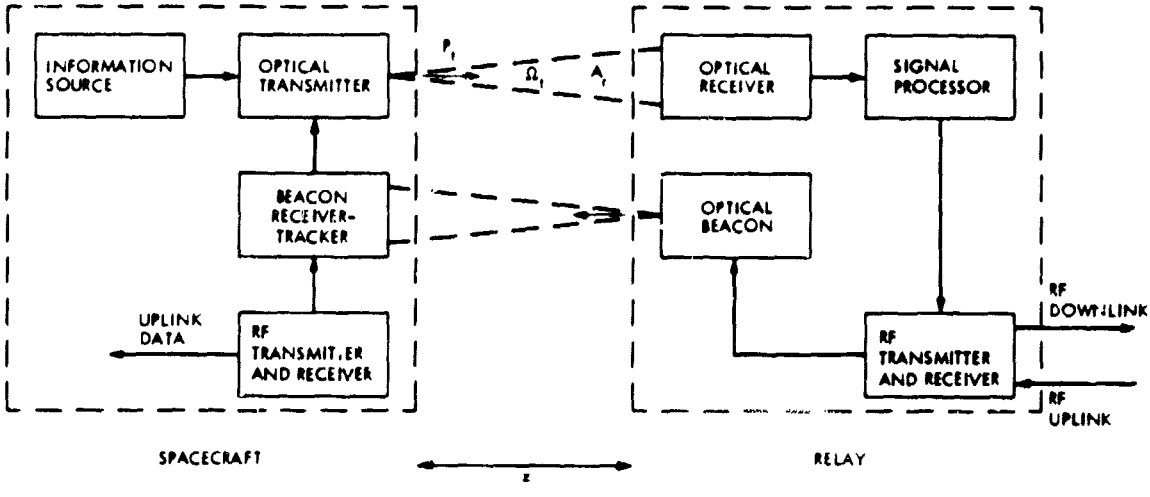

Figure 1-2. Spacecraft-Relay Subsystems: Block Diagram

power of P_t watts, the amount of optical power collected by an optical receiver with effective[1] collecting area A_r located on the beam axis in the far-field of the beam is given by

$$P_r = \frac{P_t A_r}{\Omega_t z^2} \tag{1-1}$$

where z is the distance between the transmitter and the receiver (measured along the beam axis). The beam divergence Ω_t is defined to be

$$\Omega_t = \lambda^2/A_t \tag{1-2}$$

where λ is the wavelength of the optical field. It is sometimes convenient to deal with the "planar" beam divergence θ_t defined as $\theta_t = \sqrt{4\Omega_t/\pi} = 4\lambda/\pi d_t$ where d_t is the diameter of the transmitter aperture.

The average signal count rate n_s produced at the output of a photodetector with quantum efficiency η_r is

$$n_s = \frac{\eta_r}{hf_o} P_r \tag{1-3}$$

where h is Planck's constant and f_o is the optical frequency.

Equations (1-1)-(1-3) are the basic link equations describing the capabilities of the optical link. Figures 1-3 a, b, c plot the normalized signal count rate in terms of three key parameters: the size of the transmitting optics, the transmitter power, and the link distance. Note that normalized signal count rates of roughly 10^7 photons/sec can theoretically be delivered to each square meter of relay aperture over Jupiter distances using a 1 watt source and 1-meter transmitting optics.

Background light entering the field-of-view of the optical receiver will produce noise counts, hindering the detection of the signal field. The background rate generated by a distributed source at the relay receiver with effective collecting area A_r, field-of-view Ω_r ster, and optical pre-detection filter bandwidth $\Delta\lambda$ is

$$n_b = \frac{\eta_r}{hf_o} N(\lambda)\Delta\lambda\Omega_r A_r \text{ counts/sec} \tag{1-4}$$

1. The effective collecting area is defined as the actual collecting area multiplied by the transmission factor of the optical system.

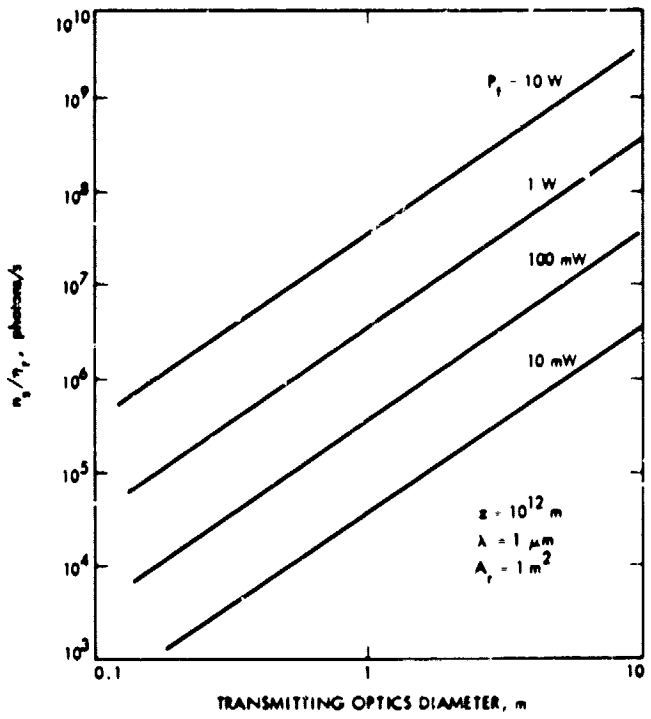

Figure 1-3a. Average Detected Signal Count Rate as a Function of Transmitting Optics Diameter

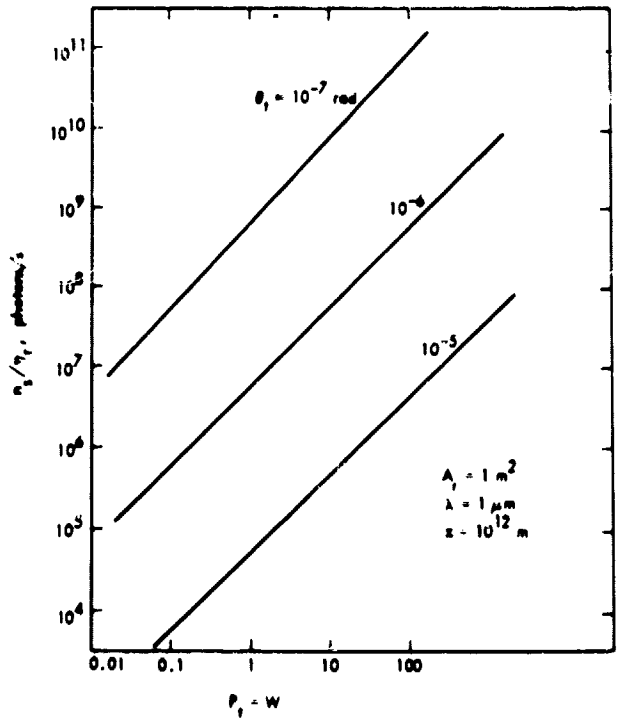

Figure 1-3b. Average Detected Signal Count Rate as a Function of Spacecraft Power Level

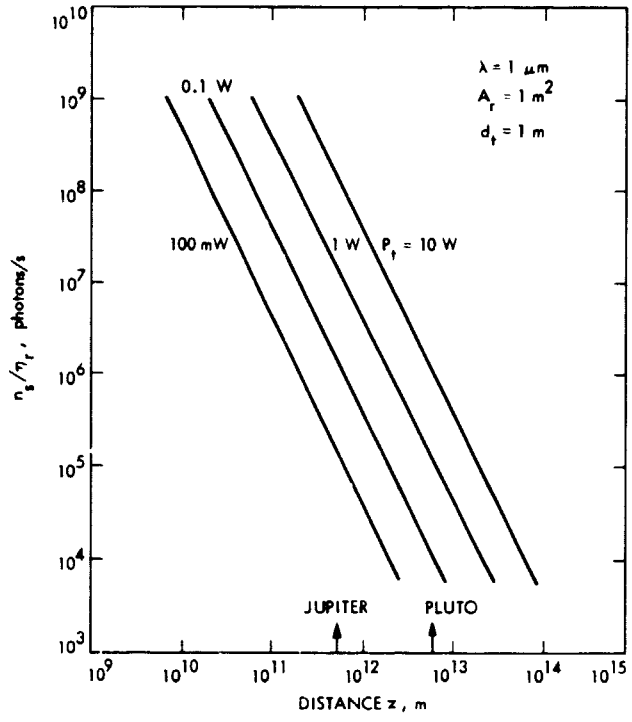

Figure 1-3c. Average Detected Signal Count Rate as a Function of Communication Link Distance

where $N(\lambda)$ is the radiance function of the background at wavelength λ. For point-source interference, such as a star, the noise count-rate is independent of the field-of-view. Figure 1-4 shows the normalized count-rate generated by some typical background sources at a relay receiver as a function of its planar field-of-view θ_r, for typical background models.

1.3 OPTICAL DATA RATES

The actual data rate (bits/sec) that can be transmitted over the optical link from spacecraft to relay will depend on the encoding format used to modulate the optical carrier. It is convenient to characterize the encoding scheme in terms of its count information rate ρ (in bits/count). The transmitted data rate R_o that can be maintained by an optical link producing n_s signal counts per second at the receiver is then

$$R_o = \rho n_s \text{ bits/sec} \qquad (1\text{-}5)$$

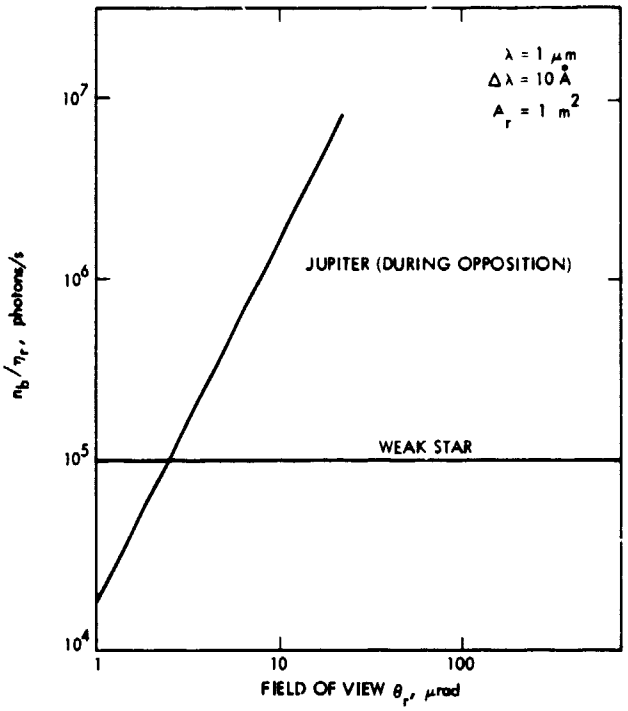

Figure 1-4. Normalized Background Count Rate as a Function of Receiver Field of View

The value for the parameter ρ depends on the modulation encoding method and on the desired bit error probability. The advantage of interpreting the data rate as in (1-5) is that it separates the transmitter design problem into a link budget design (maximizing n_s) and an encoding design (maximizing ρ).

In the following we examine several possible optical modulation techniques that could be used in a deep space mission. It is expected that initially modulation formats will be limited to pulsed intensity modulation and direct detection schemes compatible with pulsed laser operation. Here we assume that negligible background radiation reaches the photodetector; however in future studies the effects of background radiation on receiver performance should be examined.

1.3.1 On-Off Keying

In on-off keying (OOK), data is sent as binary information signified by the presence or absence of the light pulse. Let T be the pulse width and the repetition period (assumed to be equal). Assume the spacecraft optical source can deliver an average of n_s counts/sec at the relay. An on-off keyed system with equal a priori probabilities produces one bit every T sec with an average optical pulse count of $K_s/2$ counts, where

$$K_s = n_s T \quad \text{counts} \tag{1-6}$$

The system therefore operates with

$$\rho = \frac{2}{K_s} \text{ bits/count} \tag{1-7}$$

Its achievable bit error probability is that of an on-off keyed Poisson threshold test. With negligible background noise effects, the error probability has the form

$$PE = \frac{1}{2} e^{-K_s} = \frac{1}{2} e^{-2/\rho} \tag{1-8}$$

Figure 1-5 plots (1-8) as a function of ρ for an on-off keyed system.

1.3.2 Pulse Position Modulation (PPM)

In the standard PPM format data is encoded into an optical pulse placed in one of M time slots in each frame. The value of M depends on the number of slots of width τ that can be placed in each repetition period T, allowing time for pulse buildup and extinction. With a pulse count given by (1-6), the count information rate is

$$\rho = \frac{\log_2 M}{K_s} \text{ bits/count} \tag{1-9}$$

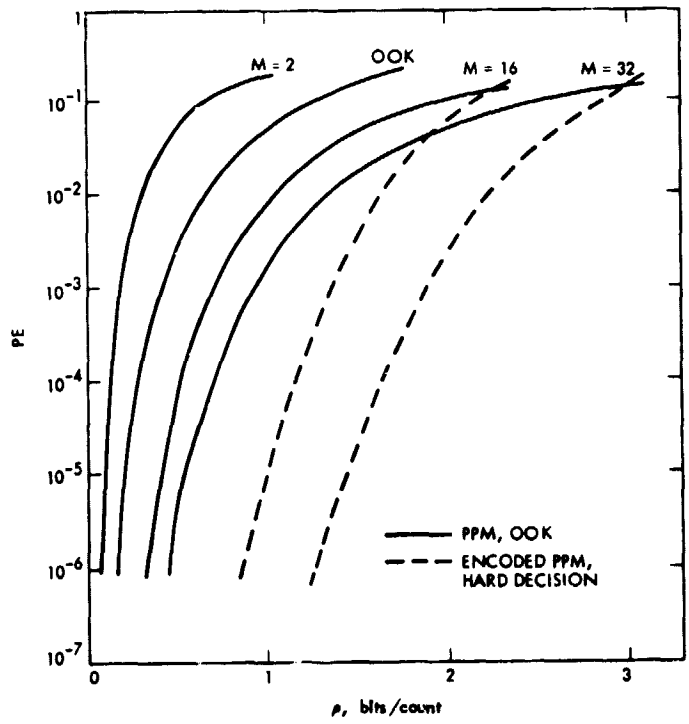

Figure 1-5. Performance Curves for Various Optical Modulation Techniques

The corresponding word error probability for the noiseless receiver is known to be

$$PWE = \frac{M-1}{M} e^{-K_s}$$

$$= \frac{M-1}{M} e^{-(\log_2 M)/\rho} \qquad (1\text{-}10)$$

$$= \frac{M-1}{M} M^{-(\log_2 e)/\rho}$$

The corresponding bit error probability PE is related to the word error probability by

$$PE = \frac{\frac{M}{2}}{M-1} PWE$$

$$= \frac{1}{2} M^{-(\log_2 e)/\rho} \qquad (1\text{-}11)$$

Equation (1-11) is also plotted in Fig. 1-5 for several values of M, as a function of ρ. At a given word error probability, ρ is increased by increasing the number of PPM slots, provided that the required value of pulse counts K_s can be maintained. For a fixed value of n_s, this improvement can only be achieved by increasing the peak power of the laser pulse, while at the same time decreasing its duration. The peak power P_p is related to the average power P_r by $P_p = P_r T/\tau$ or $P_p = MP_r$. Hence the number of slots M also determines the required peak-to-average power ratio of the spacecraft laser.

1.3.3 Pulse Encoded PPM with Hard Decision Decoding

The PPM format can be extended to include pulse encoding over multiple PPM frames, with hard decision decoding used to decode the transmitted data. An earlier study (Ref. 4) considered this format, with Reed-Solomon (RS) code sets used to form the PPM frame sequence. In this method an (N,k) RS code is used to encode M^k codewords into N PPM frames by properly locating a pulse in each frame. A hard decision decodes the signal pulse in each frame, and a word decision is made from the set of frame decisions. For this format

$$\rho = \frac{k \log_2 M}{NK_s} \text{ bits/count} \qquad (1\text{-}12)$$

and the corresponding word error probability is approximately

$$PWE \leq \sum_{j=d}^{N} \binom{N}{j} \left(e^{-K_s}\right)^{j} \left(1 - e^{-K_s}\right)^{N-j} \qquad (1\text{-}13)$$

where $d = N - k + 1$ is the code set minimum distance of the RS code. Solving (1-12) for K_s and using it in (1-13) generates PWE as a function of M and ρ. When a word error is made it is most likely made with a word located a distance d away. This means that with high probability d frame errors are made. The error probabilities associated with the individual PPM frames are identical because the RS codes are cyclic, and so the probability of any particular frame being in error, given a word error, is d/N (Ref. 5). The corresponding bit error probability is then approximately half the PPM frame error probability. Hence,

$$PE \simeq \frac{1}{2}\left(\frac{d}{N}\right) PWE \qquad (1\text{-}14)$$

For a rate 1/2 RS code set with $k = M/2$ and $N = M - 1$ and a distance of $d = M/2$ the resulting PE using the results from Ref. 4 are included in Fig. 1-5.

1.3.4 Conclusions

The conclusions from Figure 1-5 are that values of ρ much beyond one bit per count may be achieved at the expense of higher error probability, or by resorting to more complex encoding and receiver processing. It is expected that the search for convenient optical encoding procedures will be a continuing task in any data link development.

For a value of $\rho = 1$ bit/count, it can be deduced from Figure 1-3a that in the absence of pointing errors, data-rates on the order of 10^7 bits/sec can be achieved over a distance of 10^{12} meters, using 1-meter transmitting optics, a 1 watt source and a 4.5 meter receiver (assuming detector quantum efficiency of 20% and a system transmission factor of 0.8). This rate is about a hundred times higher than that achieved by present-day RF systems operating over the same range.[2] Alternatively, present RF data-rate capabilities can be extended to greater distances by the use of an optical data relay link. Figure 1-6 shows the factor by which optical relay systems can theoretically extend current RF communications distances for deep-space missions. These numbers are, of course, predicated on the idealized assumptions (negligible background radiation, perfect beam pointing and pulse timing) made in the derivation.

2. Present-day RF deep-space communications systems (such as the Voyager spacecraft in conjunction with a 64-meter receiver) can operate at roughly 10^5 bits/sec from a distance of 10^{12} meters (Ref. 11).

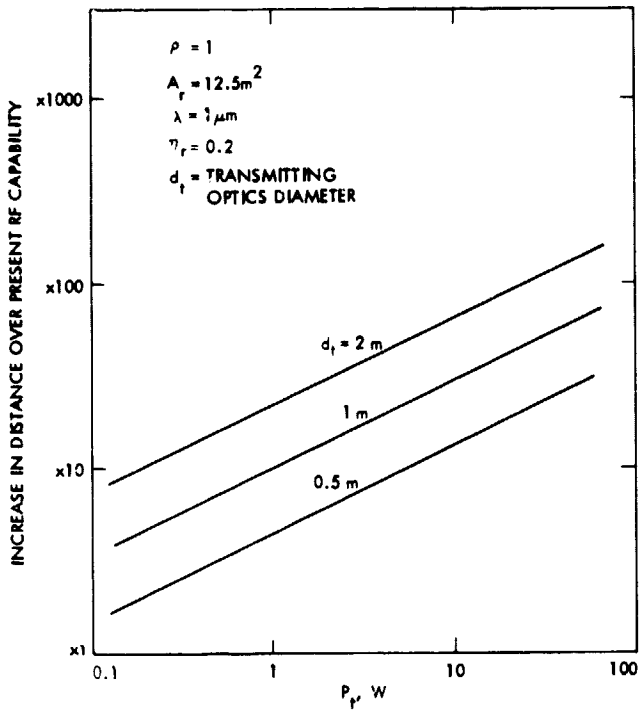

Figure 1-6. Potential Extension of Communication Range Offered by Optical Link

SECTION 2

ACQUISITION, TRACKING AND POINTING

2.1 THE POINTING PROBLEM

The use of narrow optical beams for the spacecraft-relay link introduces obvious beam pointing and tracking problems, as discussed in Ref. 1. This basic problem is summarized in Fig. 2-1. The spacecraft should transmit the narrowest possible optical beam to the relay for maximum power concentration. However, the minimal beamwidth is limited by the expected error in pointing the beam to the relay. If the pointing error is expected to be within $\pm\theta_p$ radians, then the optical beam must be large enough to encompass this $2\theta_p$ error. Hence, pointing error dictates the minimal beam size. This means that the advantages discussed in the previous sections are attainable only within the accuracy of the tracking and pointing operation.

Pointing error is determined by the entire pointing operation. The relay receiver moving with tangential velocity V_T relative to the spacecraft transmits a beacon to the spacecraft at time t_1. The spacecraft receives the beacon at time t_2, and uses the available information to determine the required point-ahead angle (magnitude and orientation) that must be used for transmitting the downlink optical beam to intercept the relay at time t_3. The required point-ahead angle depends on the orbital dynamics of the relay, and may be either computed on board the spacecraft or transmitted to the spacecraft through the auxiliary microwave link. Since the point-ahead angle is defined relative to the received beacon direction and spacecraft attitude, pointing first requires accurate beacon tracking and spacecraft attitude control for its operation.

The entire pointing operation therefore requires the spacecraft to:

(1) Acquire, locate and track the received beacon line of sight.

(2) Compute and continually update the point-ahead angle.

(3) Point the optical beam in the desired direction.

All of these operations have their own inherent errors. The combined effect of all the errors produces the total pointing error (Fig. 2-1) of the data return link. The minimal optical beam must then encompass this pointing error in order to ensure reliable communications. In the following sections we examine the principal contributions to this error.

The spacecraft optical pointing subsystem will generally have a form similar to that of Fig. 2-2. After initial acquisition the received beacon is continually processed for beam tracking. The beam tracking generates an error signal which is used to keep the receiving optics aimed at the beacon. The tracking information, in conjunction with spacecraft attitude sensing and transmitted relay location, is used to compute the point-ahead angle. The computed angle is used to gimbal the transmitting optics so as to properly point the optical data carrier.

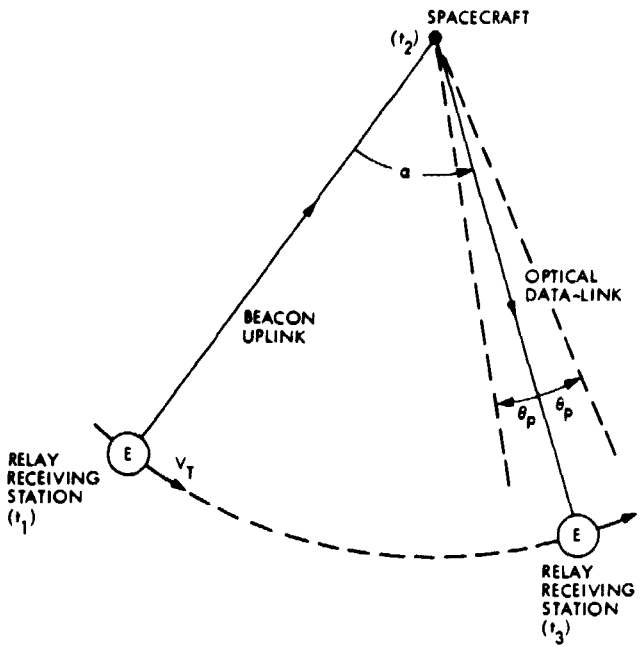

Figure 2-1. Pointing Geometry

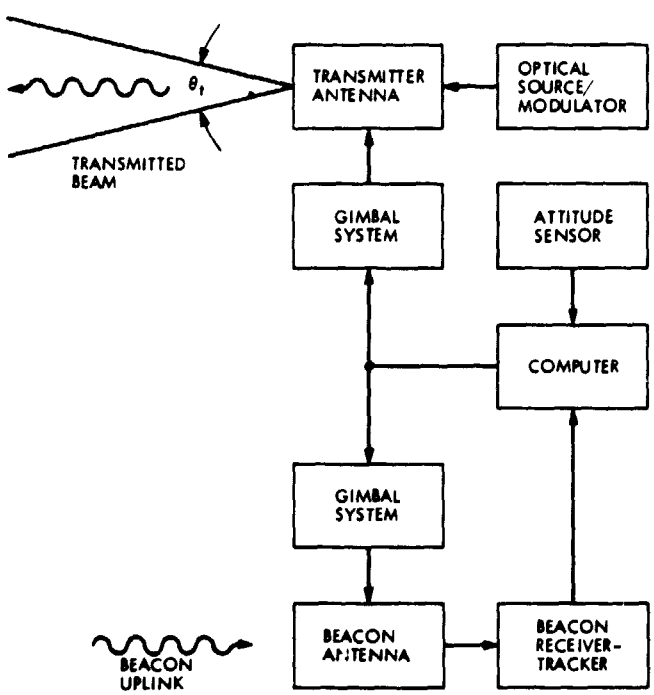

Figure 2-2. Spacecraft Optical Tracking and Pointing System

An important consideration is whether the relay-spacecraft tangential velocity V_T is significant enough to require separate receive and transmit optics at the spacecraft. If the point-ahead angle is not large, it may be possible to utilize common optics. This avoids the problem of having to transfer line-of-sight directions from one optical system to another.

2.2 SPACECRAFT-RELAY GEOMETRY

In order to discuss the pointing problem more fully, it is helpful to have a geometrical picture of the relative positions and motions of the spacecraft, the relay, and Earth. The relay is assumed to be circling Earth once every 24 hours in a geostationary orbit of radius 42,000 km. The relay's orbital path lies within the equatorial plane of Earth. Concurrently, Earth and the relay within its gravitational pull are both moving along the Earth's yearly orbit around the Sun at a radius of 1 AU (150,000,000 km). This orbit takes place in the ecliptic plane, which intersects the Earth's equatorial plane at an angle of 23 1/2°. The spacecraft is assumed to be on a journey to the outer planets or beyond (range from Earth >5 AU). Unlike the relay, it is well outside Earth's gravitational influence and it may be assumed to be executing an independent trajectory. However, during the crucial stages of its data reporting mission the spacecraft is likely to be involved in an encounter with a distant planet or other heavenly body whose gravitational influence will cause spacecraft orbital motions similar to the relay's motions under the influence of Earth.

The basic spacecraft-relay geometry is depicted in Fig. 2-3. For communication purposes it is important to know the variations of the line-of-sight vector (LOS) between the relay and the spacecraft. The direction of the LOS is conveniently specified in terms of two angles relative to the two planes in which the relay's orbital motions take place. The angle β is defined as the angle between the LOS and the ecliptic plane, and the angle δ is the angle between the LOS and Earth's equatorial plane. For missions to planets which are approximately within the ecliptic plane, β will be near 0° and δ will vary between +23 1/2° and -23 1/2°, depending on the positions of the spacecraft and Earth relative to the (fixed direction of) Earth's rotational axis (see Fig. 2-3).

2.2.1 Potential Blockage of the Spacecraft-Relay LOS

One of the advantages of a relay system compared with a direct link to Earth is that it eliminates the need for several widely distributed ground stations that must alternate coverage responsibility as the Earth's rotational motion takes turns obstructing the LOS of each station. The geostationary relay satellite is constantly within the view of a single ground station placed anywhere within its footprint. The spacecraft-relay LOS may also be subject to the same type of periodic rotational blockage by Earth as that experienced by a ground station, but the incidence and extent of these outages are reduced to insignificant levels due to the small angle subtended by Earth from the relay's position. Additional blockage by other bodies may occur during

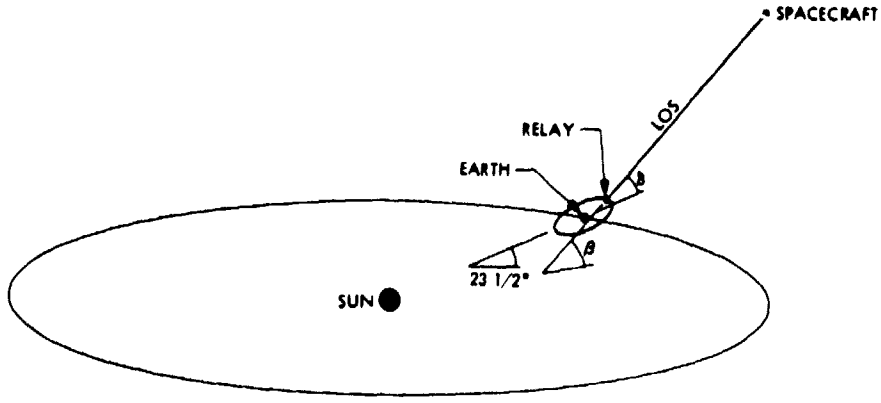

Figure 2-3. Spacecraft-Relay Geometry

an encounter, but since these effects are basically identical for relay and direct links they will not be discussed here.

The possible blockage of the spacecraft-relay LOS by Earth is analyzed with the help of Fig. 2-4. At any moment in time the Earth casts a shadow over a conical region of half-angle

$$\varepsilon \simeq R_E/R_r \simeq 9° \qquad (2\text{-}1)$$

where R_e, R_r are the radii of Earth and the relay's orbit, respectively. Thus, as long as the spacecraft-relay LOS is more than 9° outside Earth's equatorial plane (i.e., $|\delta| \geq 9°$), blockage will not occur. If the spacecraft is positioned exactly within the equatorial plane (i.e., $\delta = 0°$), the

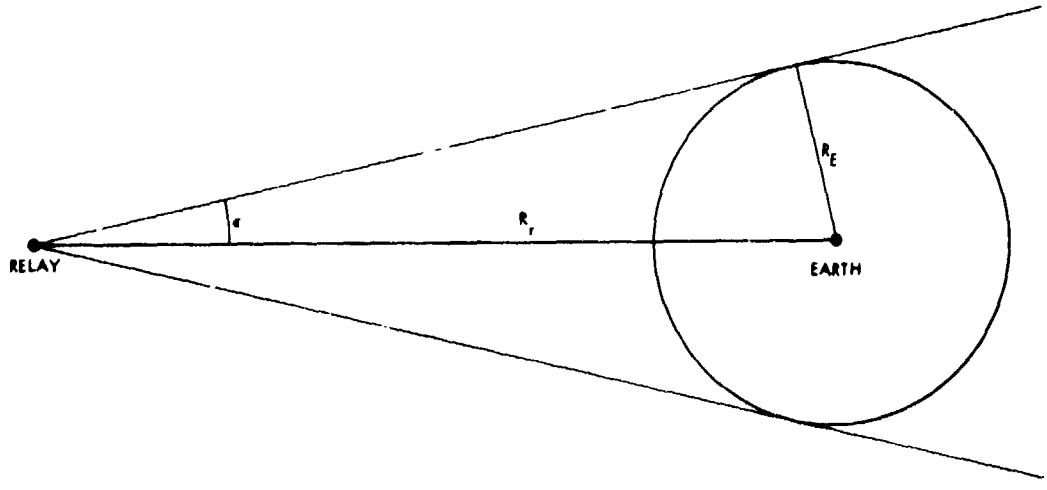

Figure 2-4. Blockage of the Spacecraft-Relay Line-of-Sight by Earth

LOS will be blocked for 18° out of every relay orbit or five percent of every 24-hour period. While this worst case outage time is small, it is probably worthwhile to eliminate it entirely by scheduling the mission at a time of year when the spacecraft-relay LOS is significantly removed from the equatorial plane.

2.2.2 Effects of Spacecraft-Relay Relative Motion

There are two main categories of effects caused by relative motion between the relay and the spacecraft. Radial motion causes a doppler shift of the optical carrier frequency. Tangential motion causes the spacecraft-relay LOS direction to change with time, and if this variation is significant relative to the optical beamwidth, a point-ahead system is required. More detailed discussion and analysis of these effects is given in Appendix B and Section 2.5.

2.3 BEAM ACQUISITION

The initial task of the spacecraft is to acquire the optical beacon from the relay (i.e., have the beacon beam impinge normal to its receiving area). Assuming the beacon is correctly pointed toward the spacecraft, the latter must orient its optics to bring the beacon arrival direction within its field of view. The spacecraft has an initial uncertainty angle for locating the beacon, and the acquisition operation reduces to a search over resolution cells within the uncertainty angle. The size of the resolution cells is equal to the spacecraft receiver field of view. This field of view must be small enough to restrict the amount of background light relative to the beacon power that will be received, in order to ensure that the beacon will be detected when it does appear in the spacecraft field of view.

The situation is depicted in Fig. 2-5, showing the uncertainty region as viewed from the spacecraft. The angular uncertainty region is assumed to encompass a square solid angle of Ω_u steradians, roughly $\theta_u \simeq \sqrt{\Omega_u}$ radians on a side. The angular position of the optical beam can be resolved to within Ω_{fv} steradians. Therefore, we can partition the uncertainty region into Ω_u/Ω_{fv} resolution cells, each cell $\theta_{fv} = \sqrt{\Omega_{fv}}$ radians on a side, and search the resulting matrix of resolution cells to locate the beacon source.

2.3.1 Acquisition with No Background and No Clutter

We first consider the case of no background noise and no external interference sources. Suppose that the count intensity of the beacon is n_s photons/second and the average number of photons generated in T seconds by a photodetector is $K_s = n_s T$. Correct acquisition occurs if the optical source generates at least one count over the proper resolution cell. The acquisition probability for this ideal case, PAC*, is

$$PAC^* = 1 - \exp(-K_s) \qquad (2\text{-}2)$$

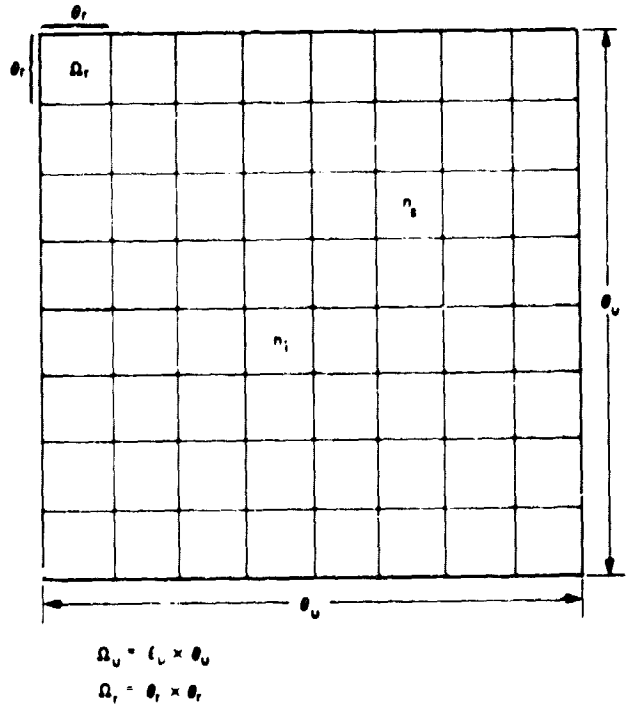

Figure 2-5. Acquisition Uncertainty Region Resolution Matrix

This ideal acquisition probability is shown in Fig. 2-6. Note that an average of at least 2.3 counts is required per observation interval in order to maintain better than 90 percent probability of acquisition.

2.3.2 Acquisition in Background Noise

When background noise is present, successful beacon acquisition requires both the integrated beacon count to be sufficiently high and the beacon count rate to be suitably high relative to the background noise rate. From Poisson detection probabilities, an acquisition probability of 0.999 in a single search scan can be achieved if the beacon count rate n_s, the background count rate n_b, and the integration time T roughly satisfy (Ref. 6, Chap. 11):

$$\frac{n_s}{n_b} \simeq 10 \qquad (2\text{-}3a)$$

and

$$n_s T \simeq 10 \qquad (2\text{-}3b)$$

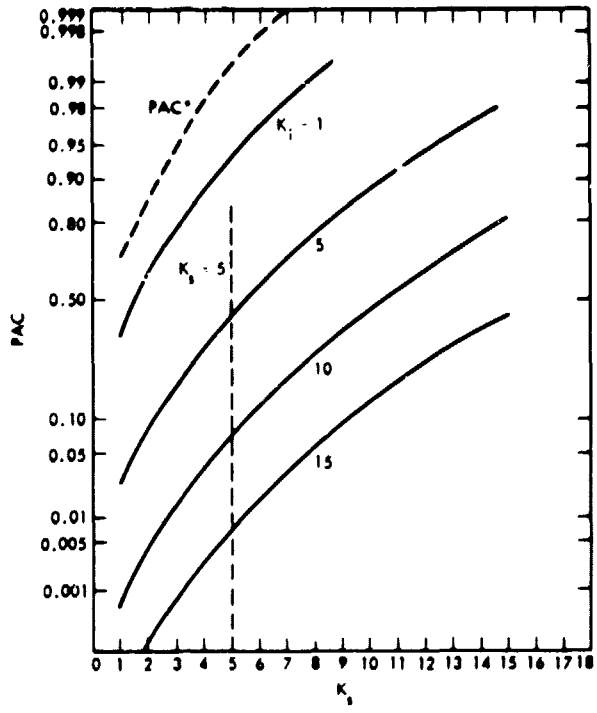

Figure 2-6. Acquisition Probability for Ideal Case and for Various Clutter Levels

If antenna or focal-plane scanning is used, the acquisition time T_{ac} is the time required to search all of the uncertainty angle Ω_u. Thus,

$$T_{ac} = \left(\frac{\Omega_u}{\Omega_{fv}}\right) T \tag{2-4}$$

As the field of view of the spacecraft receiver is reduced, less noise is received and the beacon count rate needed to produce the desired acquisition probability decreases, but the acquisition time increases. Fig. 2-7 plots equations (2-3) and (2-4) as a function of spacecraft receiver field of view, for several uncertainty beam angles, exhibiting these effects. A background model based on an illuminated Earth viewed from Jupiter at a wavelength of one micron with a 10Å bandwidth optical filter was used. If it is assumed that the beacon count produced by the relay is known, Fig. 2-7 is entered at the left ordinate, projected across the n_s curve, and the required receiver viewing angle and resulting acquisition time for the given uncertainty are read off. Conversely, for a given spacecraft view angle one can read vertically to determine the required beacon count and approximate acquisition time.

The use of (2-4) is based on acquisition using comparison tests among the integrated counts from all the uncertainty regions. This means that the total region must be scanned before an acquisition decision is made. In addition,

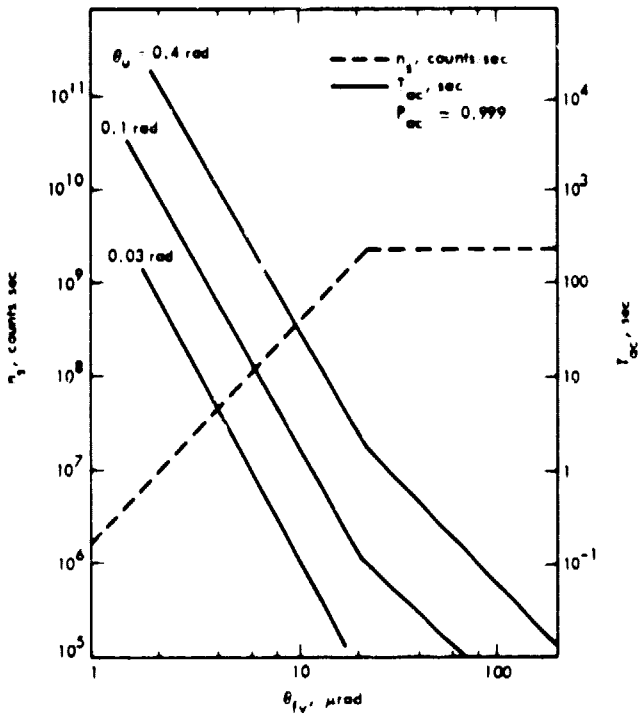

Figure 2-7. Acquisition in the Presence of Background Noise

the use of arrays (groups of photodetectors placed in the focal plane of the optical receiver) has been suggested for acquisition time reduction at the expense of increased receiver processing (Ref. 6, Chap. 11).

2.3.3 Acquisition in Clutter

The acquisition operation is severely degraded by the presence of other bright sources (stars, moon, planets, etc.) within the uncertainty field. We now consider the acquisition problem when a single interfering clutter source is included in Ω_U, along with the desired optical source (Ref. 2). (The extension to more than one interfering source is straightforward). The interference is assumed to be far enough removed from the desired source (and small enough in angular extent) to excite a different resolution cell, inducing a count intensity of n_i photons/second, and an average observed count of $K_i = n_i T$ photons over that resolution cell. The resolution cell with the greatest number of observed counts is selected. Correct acquisition takes place if the beacon generates more counts than the interference (in case of a tie, we assume the search is repeated). The probability of correct acquisition, PAC, in the presence of clutter can therefore be expressed as

$$PAC = \sum_{k=1}^{\infty} \frac{K_s^k}{k!} e^{-K_s} \left(\sum_{\ell=0}^{k-1} \frac{K_i^\ell}{\ell!} e^{-K_i} \right) \tag{2-5}$$

Figure 2-6 shows the behavior of PAC as a function of K_s for increasing values of the average interference-induced count K_i. It is apparent that weak interference ($K_i << K_s$) has no appreciable effect on the acquisition probability, but PAC deteriorates rapidly in the presence of strong interference ($K_i \geq K_s$).

One rather obvious solution to the interference problem is therefore to increase the source power until n_s becomes much greater than n_i, while holding the observation time constant. Unfortunately, this solution may not always be practical, due to the increased power consumption required.

If the beacon and interference count intensities are comparable, but $n_i < n_s$, then PAC can be improved by increasing the observation interval, as shown in Fig. 2-8. When $(n_i/n_s) < 1$, PAC shows some improvement with increasing T, but the rate of improvement decreases as (n_i/n_s) approaches unity. For $(n_i/n_s) = 1$, the acquisition probability cannot be improved by increasing T, while for $(n_i/n_s) > 1$, increasing the observation time only increases the probability of mistakenly acquiring the interference. This behavior is clearly illustrated by the curves corresponding to $(n_i/n_s) = 2$ and 4 in Fig. 2-8.

We see, therefore, that it becomes difficult to achieve high acquisition probabilities by increasing the source power or the observation time, in the presence of intense clutter. Some additional advantage may be gained by a combination of the two techniques; that is, by increasing the source power to drive α below unity, and simultaneously increasing the observation time.

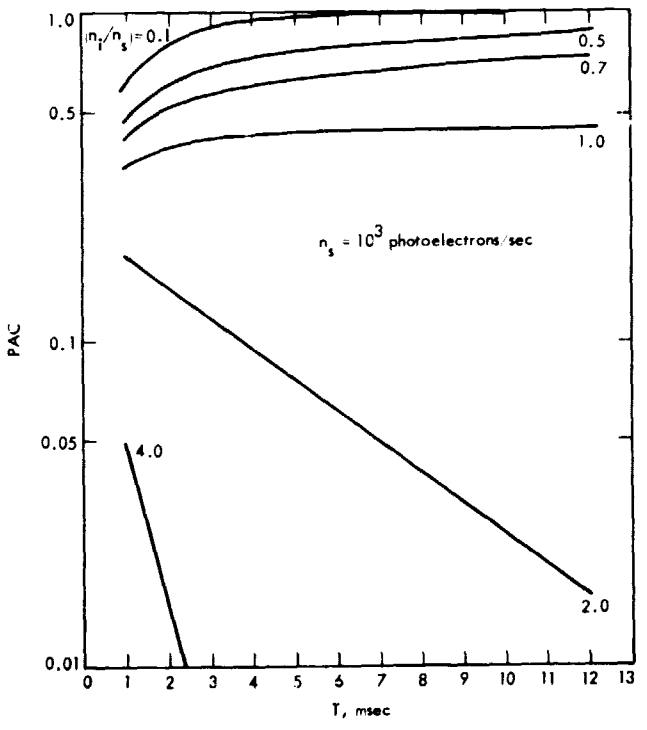

Figure 2-8. Acquisition Probability in Clutter, as a Function of the Length of the Observation Interval

2.3.4 Pulsed Beacon Acquisition

An alternate method for improving acquisition is by the use of a pulsed beacon. Here the beacon is repeatedly pulsed on and off, while the required timing information may be simultaneously transmitted to the spacecraft over a separate RF channel. (The requirement to transmit timing information to the spacecraft should not overburden the RF uplink, since optical acquisition is inherently a relatively short-duration operation.) Beacon timing can also be derived from standard pulse acquisition and temporal tracking subsystems operating on the actual received beacon waveforms.

We assume that the beacon laser generates a periodic beacon pulse train, while maintaining constant average power as shown in Fig. 2-9. The counts generated at the spacecraft by the beacon now appear concentrated in narrow, high count intensity pulses of duration τ'-seconds, at regular T'-second intervals. In order to maintain the average beacon count rate at n_s counts/seconds, the beacon count rate during each pulse time must be κn_s counts/second, where $\kappa = T'/\tau'$ is the pulse compression factor. A total of $N = T/T'$ such pulses are observed during the T-second total observation interval. The interference count rate remains n_i counts/second, uniformly distributed in time.

The timing information can be used to define τ-second observation windows around each τ'-second pulse. Note that while the minimum value of τ is τ', this limit can only be achieved with perfect timing. In general, the duration

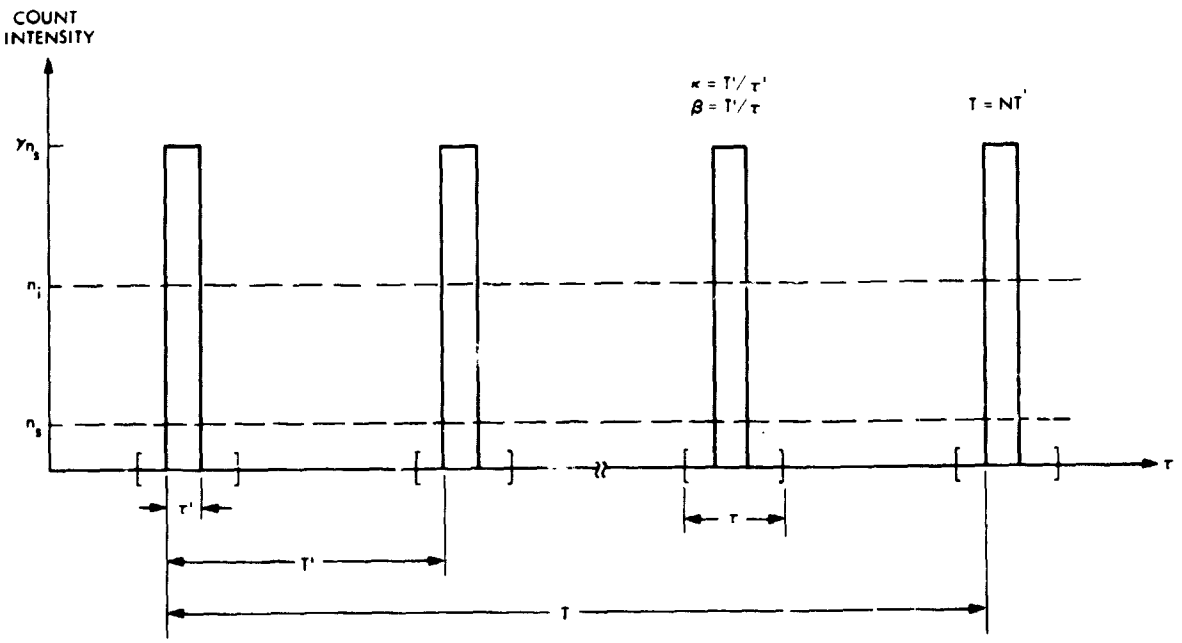

Figure 2-9. Temporal Distribution of Count Intensities for a Pulsed Beacon Source

of the observation window τ would be much greater than τ' in order to mask the effects of timing uncertainties.

The average counts due to beacon and interference in the pulsed system are

$$K_s^p = N\kappa n_s \tau' = n_s T = K_s \tag{2-6a}$$

$$K_i^p = N n_i \tau = n_i T \left(\frac{\tau}{T'}\right) = K_i \left(\frac{\tau}{T'}\right) \tag{2-6b}$$

We observe that the interference counts are effectively reduced from those for the non-pulsed system by the ratio τ/T', which is related to the accuracy of the timing information transmitted to the spacecraft. Defining the observation compression factor as $\beta = T'/\tau$, we write the average interference counts in the pulsed system as $K_i^p = K_i/\beta$. The interference suppression capability of the pulsed system is therefore determined by the system parameter β. With present day Q-switching technology and current RF timing capabilities, maximum values of β on the order of a few hundred appear feasible.

The improved performance of the pulsed system is shown in Fig. 2-10, which shows the acquisition probability PAC as a function of β at the fixed value $K_s = 5$, for various K_i corresponding to high intensity interference. The upper bound on acquisition probability, PAC* = 0.9933, is also shown for comparison. Figure 2-10 should be compared with Fig. 2-6 (at $K_s = 5$) for a direct measure of the improvement provided by the pulsed system. Without pulsing ($\beta = 1$), the acquisition probability corresponding to $K_s = 5$ and $K_i = 10$ is PAC = 0.074, while even modest compression ratios ($\beta > 20$) yield PAC = 0.98. With improved timing ($\beta > 100$), reasonable acquisition probabilities can be obtained, even in the presence of extremely intense interference, as demonstrated by the curves corresponding to $K_i = 20$, 50 and 100 in Fig. 2-10. Similar improvements over continuous intensity systems can be demonstrated at other values of K_s as well.

We see therefore that in the presence of strong clutter, acquisition probabilities can be improved either by increasing the average beacon power, or by pulsing the beacon (with a constant average power constraint) and relying on timing information transmitted in a separate channel to reduce the interfering counts. Both these techniques tend to increase system cost and complexity, and therefore it may be desirable to employ an optimum combination of both techniques in order to improve acquisition performance. Figure 2-11 shows graphs of constant PAC over the (β, K_s) plane. Each graph represents the locus of points corresponding to a constant acquisition probability in the presence of interference. It is apparent that for any interference level K_i, a continuum of points can be found in the (β, K_s) plane to achieve any desired level of PAC. The two system parameters β and K_s can therefore be traded off on the basis of cost and complexity while maintaining the required level of acquisition performance.

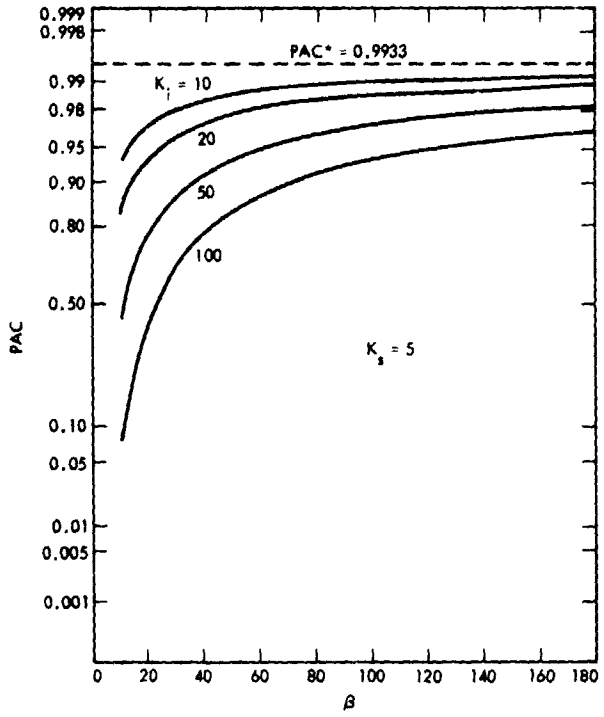

Figure 2-10. Acquisition Probability as a Function of the Observation Compression Factor for a Pulsed System

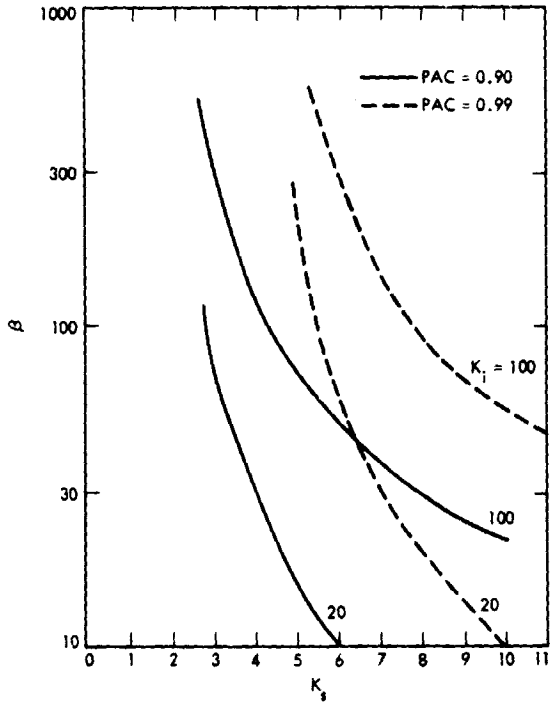

Figure 2-11. Acquisition Probability Contours for a Pulsed System, as a Function of the Observation Compression Factor and the Average Signal Count

2.4 BEAM TRACKING

After beacon acquisition the spacecraft must continuously track the LOS (line-of-sight vector) of the arriving beacon field, since the latter may vary due to relative motion. The standard procedure for tracking the arriving beacon is to focus the acquired field onto the crosshairs of a quadrant detector and use azimuth and elevation error signals to control the gimballing of the receiver optics, keeping the LOS normal to the quadrant. If the LOS is normal to the quadrant, then the required point-ahead is a fixed (computable) angle from the LOS. Hence LOS tracking errors will convert directly to point-ahead errors even with precise point-ahead computation.

Tracking error studies associated with gimbal-controlled positioning loops have been previously reported (Ref. 7). A detailed analysis of the beam tracking problem is presented in Appendix A. Summary features are described below. For purposes of analysis, the system is similar to a phase lock tracking loop. The primary tracking errors are caused by motion of the LOS, gimbal vibrations, noise, and clutter.

The LOS motion of the relay should be minimal when viewed from a spacecraft in deep space. Since the Earth's orbital velocity is 30 km/sec, the maximum angular rotation rate of the relay relative to a spacecraft at $Z = 10^{12}$ meters is roughly[3]

$$\dot{\theta} \simeq 0.03 \ \mu\text{rad/sec} \tag{2-7}$$

which is negligible for LOS tracking. Hence, it is expected that tracker bandwidths will be set by the internal vibrations of the receiver and by the detector noise rather than by relay dynamics.

The total rms tracking error due to detector noise is given by (Appendix A, Equation A-34)

$$\psi_{rms} = \frac{1.4 \frac{\lambda}{D}}{\sqrt{\gamma}} \tag{2-8}$$

where λ is the optical beacon wavelength, D is the spacecraft receiver diameter, and γ is the loop SNR approximated by

$$\gamma \simeq \frac{16}{3\pi} \frac{n_s}{B_L} \tag{2-9}$$

[3] Approximate distance to Jupiter.

Here n_s is the average beacon count and B_L is the tracking loop equivalent noise bandwidth. Note that for $n_s = 10^5$ counts/sec, a 1-kHz bandwidth, and a 1-meter spacecraft receiver at 1 micron, an rms tracking error of roughly 0.1 microradian occurs. Equation (2-9) assumes the background and receiver thermal noise count is negligible relative to the beacon count (quantum limited operation). If these noise contributions are important, they combine to reduce the loop SNR (and thereby increase the rms error) according to Eq. (A-29).

The rms tracking error due to gimbal variations is given by (A-35)

$$\sigma_g = \left[\frac{1}{2\pi} \int_{-\infty}^{\infty} S_g(\omega) \left| 1 - H(\omega) \right|^2 d\omega \right]^{1/2} \tag{2-10}$$

where $S_g(\omega)$ is the spectrum of the structural vibrations, and $H(\omega)$ is the loop gain function of the linearized loop model. Equation (2-10) indicates that the frequency components of the vibration within the loop bandwidth (range of ω where $H(\omega) \approx 1$) will be tracked out by the loop, while those outside this bandwidth will contribute directly to tracking errors. This means the tracking loop bandwidth should be large enough to exceed the significant frequencies of the expected gimbal vibration spectrum.

Bias error due to detector imbalance and background clutter may be the severest hindrance to accurate beam tracking. These effects add dc offsets to the loop control signals that can steer the receiver from the LOS (see Section A.3.3 of Appendix A). Detector imbalance can often be compensated, although the imbalance is related to the detector gain and dark current, both of which are random and can change in time. Clutter effects can be the most severe. Consider the situation depicted in Fig. 2-12. The relay is shown in synchronous orbit around the Earth. In situation (a) it is evident that a spacecraft receiver field of view of less than 30 μrad will not see the Earth, while receiving the relay beacon. However, in situation (b) the Earth's illumination will appear as clutter, and can possibly capture the tracking operation. Unless the relay beacon count dominates over this clutter, the bias offset effect may have to be seriously considered in the evaluation of the tracking accuracy.

The bias error caused by clutter is summarized by two equations (one for azimuth and one for elevation) of the form (see A-46)

$$\frac{n_s}{n_s + n_c} S(\psi_s) = - \frac{n_c}{n_s + n_c} S(\psi_c) \tag{2-11}$$

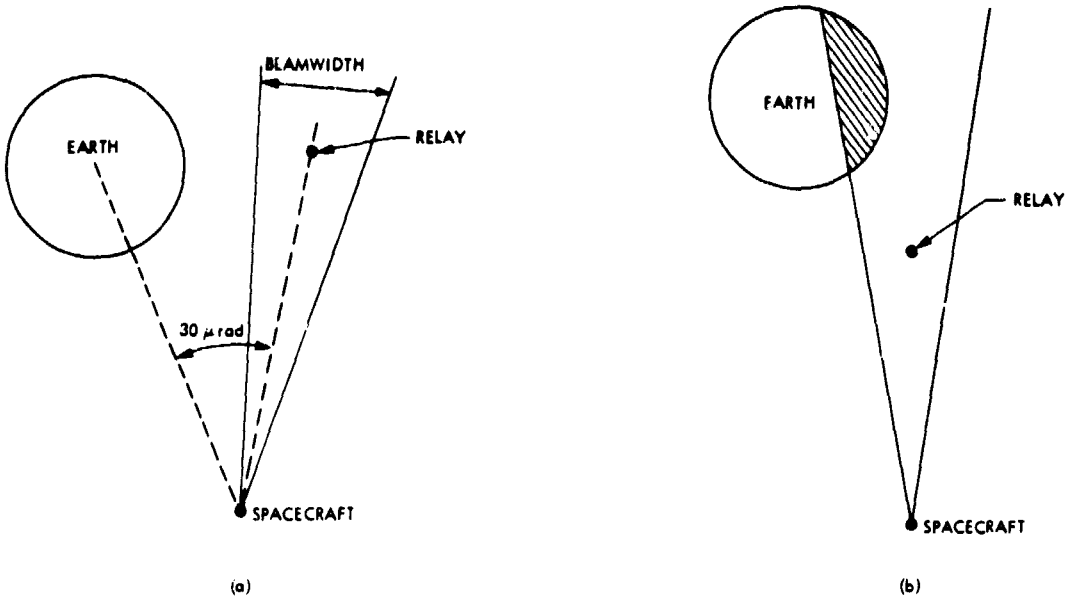

Figure 2-12. Tracking in the Presence of Clutter

Here n_s and n_c are the average beacon counts due to source and clutter respectively, $S(\psi)$ is the detector error characteristic (see Eq. A-18 and Fig. A-3), ψ_c is the angle of the clutter centroid (relative to the tracker) and ψ_s is the bias error in tracking the true source. In general, the shape of the clutter is not important, just its total power level n_c and centroid angle ψ_c. To the extent that the error characteristic $S(\psi)$ is linear, (2-11) implies that the clutter causes a bias error proportional to its relative intensity and separation from the source. If the clutter is far removed from the source, the function $S(\cdot)$ saturates and the resulting nonlinearity causes the bias error to be less than proportional to the source-clutter separation as long as $n_c < n_s$.

If clutter and detector imbalance appear to be a serious problem in optical relay tracking, the use of modulated beacon signals should be investigated as alternative designs for clutter suppression. Modulating the beacon intensity (e.g., pulsing or sinusoidally varying) at the relay gives the photodetected position error signal frequency characteristics that allow discrimination against the slowly varying clutter, similar to the pulsing advantage described in acquisition.

2.5 POINT-AHEAD

The spacecraft must point ahead by the proper angle and direction for the data return link. The required angle is given approximately by

$$\alpha = \frac{2V_T}{c} \qquad (2\text{-}12)$$

where V_T is the average tangential velocity in Fig. 2-1 and c is the speed of light. This angle is independent of the spacecraft-relay separation distance z because, although angular changes vary inversely with z, the round trip light time increases proportionately with z. For velocities at Earth-orbiting speeds, point-ahead angles up to approximately 200 μrad may be expected. For beamwidths on the order of 1-10 μrad, the point-ahead angle may therefore be many multiples of the beamwidth.

It is expected that in initial system concepts the required point-ahead will be transmitted as commands from the relay or ground station through the RF or microwave links. The point-ahead accuracy will therefore depend on how well the ground station can predict the instantaneous V_T and how accurately and how often it is transmitted to the spacecraft. If the spacecraft obtains V_T with a total error of ΔV_T m/sec, then a pointing error of

$$\Delta\alpha = \frac{2(\Delta V_T)}{3 \times 10^8} \text{ radians} \qquad (2\text{-}13)$$

will occur. Operation with less than one microradian point-ahead angle error requires tangential velocity accuracy within 150 meters/second. Present DSIF capability in measuring V_T is well below 50 meters/second, so the primary concern is the accuracy to which the true tangential velocity can be decoded at the spacecraft, considering quantization and data errors.

In addition to the point-ahead angle magnitude in (2-12), the orientation angle of the point-ahead must be known. Since this orientation angle is with respect to the spacecraft attitude, errors in attitude control will translate directly to pointing errors. The overall effect of an orientation angle error is to decrease the allowable point-ahead error magnitude $\Delta\alpha$ in (2-13).

2.6 OTHER DOWNLINK BEAM POINTING ERRORS

After the LOS has been tracked and the point-ahead angle determined, the downlink optics must point the return data beam to the proper position. The accuracy with which the optics can be pointed in the desired direction depends on the following factors:

(1) Attitude reference errors in the spacecraft. In order to point, the spacecraft must establish an attitude reference. This is generally accomplished either by a gyro-stabilized platform or via star and sun sensors. Gyro systems suffer from inherent drift effects that must be continually recalibrated. Star sensing requires tracking subsystems to align the spacecraft axis.

(2) Mechanical and structural variations. Inherent vibrations, material stress and component disturbances cause the axis of the spacecraft to become misaligned. The mechanical tolerances must be accounted for in error studies.

(3) Boresight errors. The transmitting optics and gimbals produce errors in the ability to aim a narrow beam in the exact direction required. This problem is avoided if the received beacon and transmitted data use common optics, but must be considered when separate subsystems are used.

Although the contributions to the above error sources may be relatively small, the primary difficulty is that these errors are open loop errors which cannot be corrected unless the entire pointing operation is closed around the spacecraft receiver. This can be achieved by monitoring the received optical beam and transmitting pointing corrections to the spacecraft. The magnitude of these error effects and the advantages of closing the entire pointing operation will have to be further investigated.

Reported results to date indicate that sub-microradian pointing accuracies can be achieved (Ref. 8). Total dynamic errors due to structural vibration, gimbal control, torque motor noise, simulated relative motion, boresight misalignment and detector noise can be kept below 0.60 microradians rms. These preliminary results indicate that accurate pointing of microradian transmitter beams are within the capabilities of present-day technology.

2.7 THE EFFECTS OF POINTING ERRORS ON COMMUNICATION PERFORMANCE

In the previous sections, errors in attempting to point the spacecraft optical transmitter toward the relay receiver were investigated. In this section we evaluate the effect of such pointing errors on the performance of the optical communication link (Ref. 3).

Consider the model in Fig. 2-13. The optical receiver at the relay transmits an optical beacon toward the spacecraft, whose trajectory is assumed to be known with great accuracy. An optical tracking subsystem aboard the spacecraft makes use of trajectory and geometry information (possibly transmitted up by means of the optical beacon, or by means of an auxiliary RF link) to compute the required point-ahead angles. At some time t_o, the spacecraft begins to transmit a modulated optical beam toward the optical relay receiver. The transmitted beam reaches the center of the receiver aperture at some later time t_1, after propagating a total distance $z = c(t_1 - t_o)$ from the transmitter to the receiver (c is the speed of light in vacuum). The intensity of the received field is reduced from the transmitted intensity by a propagation loss proportional to $1/z^2$. With imperfect pointing, the received field intensity is further reduced because the receiving aperture does not intercept the center of the transmitted optical beam.

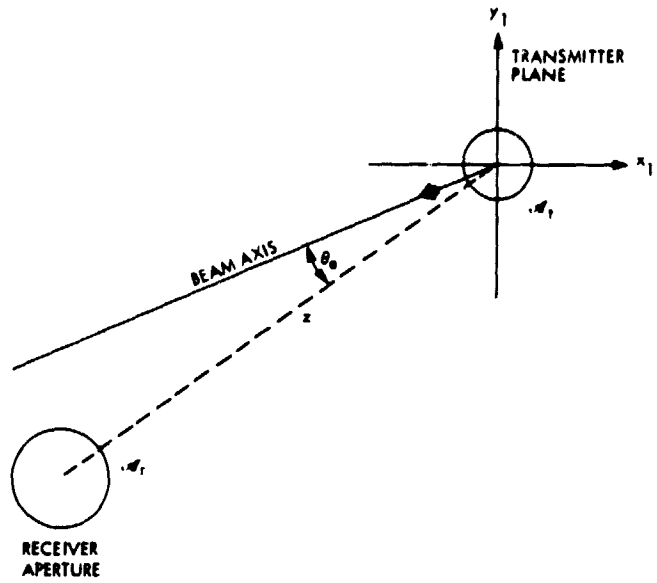

Figure 2-13. Optical Field Propagation Geometry

2.7.1 The Received Field

Consider the field propagation model associated with Fig. 2-13. A circular transmitter aperture A_t is illuminated by a normally incident optical field $U_1(t;\ x_1,\ y_1)$, where $(x_1,\ y_1)$ denote coordinates in the transmitter plane. For analytical convenience we assume that this field is a temporally modulated plane wave, modeled as

$$U_1(t;\ x_1,\ y_1) = \begin{cases} U_1(t); & x_1^2 + y_1^2 \leq \left(\frac{d_t}{2}\right)^2 \\ 0 \quad ; & x_1^2 + y_1^2 > \left(\frac{d_t}{2}\right)^2 \end{cases} \tag{2-14}$$

where d_t is the diameter of the transmitter aperture. The receiver aperture A_r is located a distance z from the transmitter at an angular position θ_e relative to the axis of the transmitted beam (see Fig. 2-13). Under the Fraunhofer (or "far-field") approximation, the optical field amplitude $U(t;\ z,\ \theta_e)$ at the receiver is given by

$$\begin{aligned} U(t;\ z,\ \theta_e) &= A_t\ U_1\left(t - \frac{z}{c}\right) f(z)\ G\left(\frac{\pi d_t}{\lambda} \sin\theta_e\right) \\ &\approx A_t\ U_1\left(t - \frac{z}{c}\right) f(z)\ G\left(\frac{\pi d_t}{\lambda}\theta_e\right) \text{ for small } \theta_e \end{aligned} \tag{2-15}$$

where

$$f(z) = \frac{e^{j2\pi z/\lambda}}{j\lambda z} \tag{2-16}$$

$$G(\zeta) = \frac{2J_1(\zeta)}{\zeta} \tag{2-17}$$

and $J_1(\cdot)$ is the Bessel function of order one. The normalized amplitude gain function $G(\zeta)$ is the normalized diffraction pattern (Airy disk) of the transmitter aperture. The amplitude gain function $G(\zeta)$ and the intensity gain function $G^2(\zeta)$, are shown in Fig. 2-14. Note that the first zero occurs at $\zeta = 3.82$, clearly defining the dimensions of the main lobe.

In writing Eq. (2-15) we have assumed that the dimensions of the receiver aperture A_r are small enough compared to the beam dimension that amplitude and phase variations over the receiver aperture can be ignored (this assumption is certainly true for optical communications systems operating over interplanetary distances when the dimensions of the receiver aperture are on the order of meters). The receiver effectively samples the optical field at the point (z, ϑ_e).

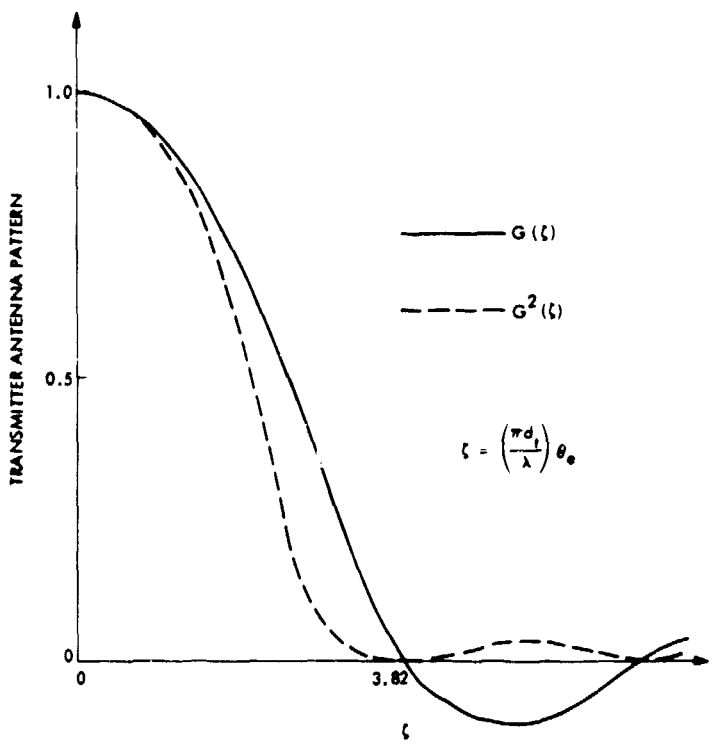

Figure 2-14. Amplitude and Intensity Patterns Generated by a Uniformly Illuminated Circular Transmitter Aperture

The temporal component of the transmitted field is defined by

$$U_1(t) = \frac{U_1}{\sqrt{A_t}}\, m(t)\, \exp\left[j\left(\omega t + \phi_1(t)\right)\right] \tag{2-18}$$

where $U_1/\sqrt{A_t}$ is a normalized field amplitude, $m(t)$ is a modulating waveform ($|m(t)| \leq 1$), ω is the radian frequency of the optical carrier, and $\phi_1(t)$ is a random phase process associated with the optical source. We can interpret the normalized amplitude $U_1/\sqrt{A_t}$ as that constant field amplitude which generates an average transmitted photon rate of $n_s = U_1^2/h\nu$ photons/second (if $|m(t)| = 1$), independent of the area of the transmitting aperture (here h is Planck's constant, and $\nu = \omega/2\pi$ is the optical carrier frequency).

2.7.2 Pointing Error Model

The total angular pointing error θ_e is conveniently decomposed into "azimuth" and "elevation" errors θ_z, θ_ℓ. If the errors are small, the azimuth and elevation components are approximately orthogonal and we can write

$$\theta_e \simeq \left[\theta_z^2 + \theta_\ell^2\right]^{1/2} \tag{2-19}$$

We shall assume that θ_z and θ_ℓ are stationary, independent random processes with mean values η_z and η_ℓ, and variances $\sigma_z^2 = \sigma_\ell^2 = \sigma^2$, respectively. The mean pointing errors could be the result of computational errors or mechanical misalignment, while the random component might correspond to tracking errors due to noise within the spatial tracking loops.

The analysis becomes somewhat tractable if we additionally assume that θ_z and θ_ℓ are Gaussian random processes. The Gaussian assumption is accurate if the uplink beacon is tracked by wideband uncoupled tracking loops operating in their linear region, driven by additive Gaussian noise. Suppressing the time dependence for notational simplicity, the joint probability density of the independent Gaussian random variables θ_z and θ_ℓ is given by the expression

$$p(\theta_z, \theta_\ell) = \frac{1}{2\pi\sigma^2} \exp\left[- \frac{(\theta_z - \eta_z)^2 + (\theta_\ell - \eta_\ell)^2}{2\sigma^2}\right] \tag{2-20}$$

The density of θ_e can be determined by a straightforward transformation of (2-20), yielding the Rice density

$$p(\theta_e) = \frac{\theta_e}{\sigma^2} \exp\left[- \frac{1}{2\sigma^2}\left(\theta_e^2 + \eta_e^2\right)\right] I_0\left(\frac{\theta_e \eta_e}{\sigma^2}\right) \tag{2-21}$$

where $\eta_e = (\eta_z^2 + \eta_\ell^2)^{1/2}$. This is the probability density of the instantaneous random pointing error on the spacecraft-relay optical carrier.

2.7.3 Effects on the Error Probability

Let us consider the effects of pointing errors on a direct detection optical link, assuming that the relay receiver is observing the M-ary PPM signal set defined in Section 1. The exact performance of M-ary PPM receivers in the presence of background radiation has been studied elsewhere (Ref. 6, Ch. 8). Here we shall assume that the effects of background radiation are negligible, and concentrate only on the effects of random pointing errors on receiver performance. From (1-10), the PPM symbol error probability can be expressed as

$$PWE = \frac{M-1}{M}\,\varepsilon \tag{2-22}$$

where

$$\varepsilon = \exp\left[-K_s\right] \tag{2-23}$$

and K_s is the average signal count per PPM symbol in the absence of pointing errors. For pulses that are much narrower than the correlation time of the pointing error process, the average pulse count, conditioned on a given pointing error θ_e, can be related to the received field as

$$\begin{aligned} K_s(\theta_e) &= \left(\frac{\eta_r}{h\nu}\right) \iint_{A_r} \left[\int_0^\tau |U(t;\,\theta_e)|^2\,dt\right] dx\,dy \\ &= \left(\frac{\eta_r}{h\nu}\right)\left(\frac{U_1^2\,A_r}{\Omega_t\,z^2}\right) G^2\left(\frac{\pi d_t}{\lambda}\,\theta_e\right) = K_s\,G^2\left(\frac{\pi d_t}{\lambda}\,\theta_e\right) \end{aligned} \tag{2-24}$$

Here τ is the pulse duration, and $\Omega_t = \lambda^2/A_t$ is the divergence of the transmitted beam, measured in steradians.

Whenever only a pointing offset is present ($\theta_e = \eta_e$), the erasure probability reduces to

$$\varepsilon = \exp\left[-K_s\,G^2\left(\frac{\pi d_t}{\lambda}\,\eta_e\right)\right] \tag{2-25}$$

This erasure probability is shown in Fig. 2-15 as a function of the normalized pointing offset $\eta_o = (\pi d_t/\lambda)\ \eta_e$, for several values of K_s. In these units, a normalized value of $\eta_o = 3.82$ corresponds to the planar half-angle of the main lobe. Recall that in typical applications $(\lambda/\pi d_t) \approx 10^{-6}$, which means that typical beam half-angles are on the order of microradians. The points where $\varepsilon = 1$ correspond to the zeroes of the main antenna pattern.

Whenever the pointing errors have a random component as well as a mean offset, the symbol error probability is obtained by averaging the conditional error probability over the density of the pointing error:

$$\varepsilon = \int_0^\infty \exp\left[-K_s(\theta_e)\right] p(\theta_e)\ d\theta_e \qquad (2\text{-}26)$$

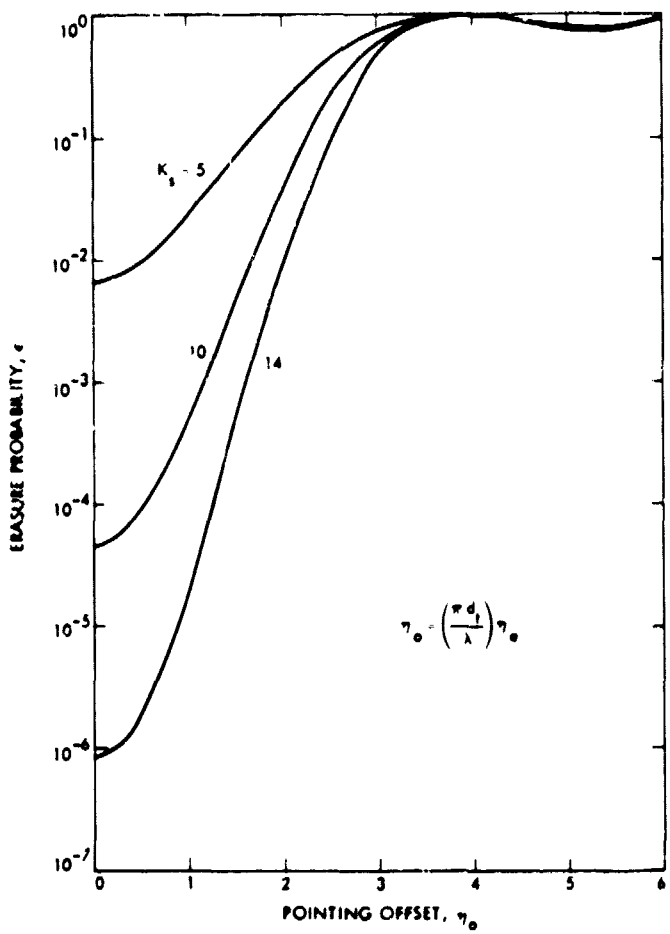

Figure 2-15. Erasure Probability in the Presence of a Mean Pointing Offset

(This expression is accurate as long as the Gaussian approximations for θ_z and θ_ℓ are valid.)

For the pointing error density of (2-21) the erasure probability becomes

$$\varepsilon = \frac{1}{\sigma^2} \int_0^\infty \theta_e \exp\left[-K_s\, G^2\left(\frac{\pi d_t}{\lambda}\,\theta_e\right) - \frac{\theta_e^2 + \eta_e^2}{2\sigma^2}\right] I_0\left(\frac{\theta_e \eta_e}{\sigma^2}\right) d\theta_e \qquad (2\text{-}27)$$

The effects of random pointing errors on the erasure probability are shown in Figs. 2-16a,b,c. (Numerical integration of Eq. (2-27) was employed to obtain these graphs.) For a given K_s, the erasure probability is shown as a function of the normalized pointing offset $\eta_o = (\pi d_t/\lambda)\eta_e$ for various values of the normalized variance $\sigma_o^2 = (\pi d_t/\lambda)^2\sigma^2$. Note that for low values of K_s ($K_s \leq 5$) the effects of pointing errors become much less pronounced, suggesting that under these conditions the requirements on pointing accuracy can be relaxed.

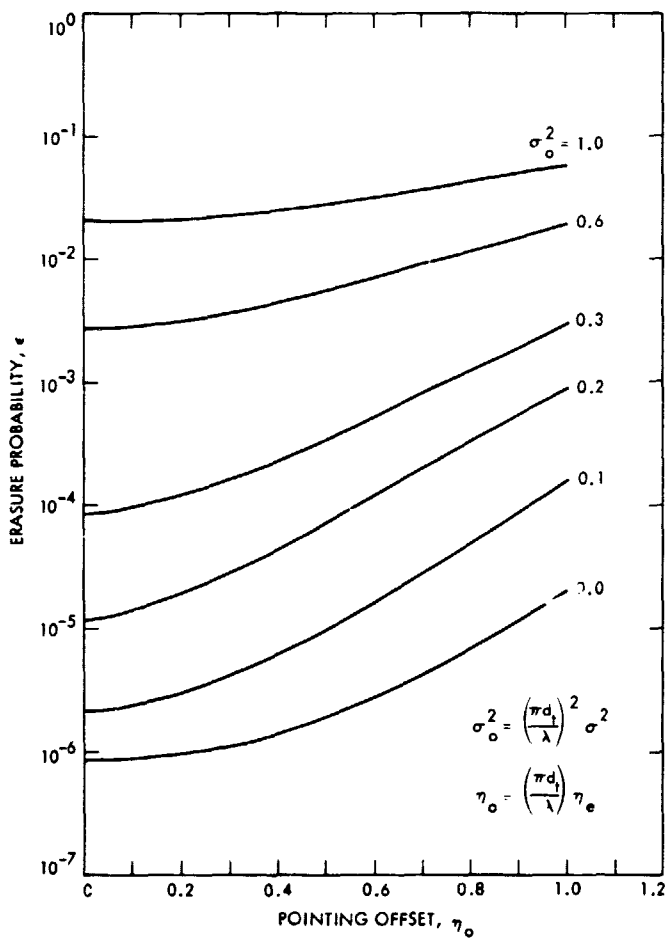

Figure 2-16a. Erasure Probability in the Presence of Random Pointing Errors: Average Signal Count = 14

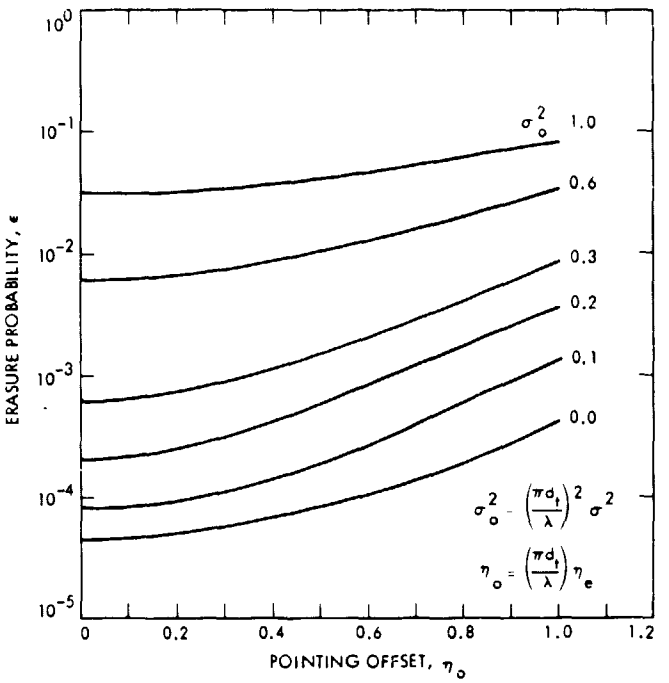

Figure 2-16b. Erasure Probability in the Presence of Random Pointing Errors: Average Signal Count = 10

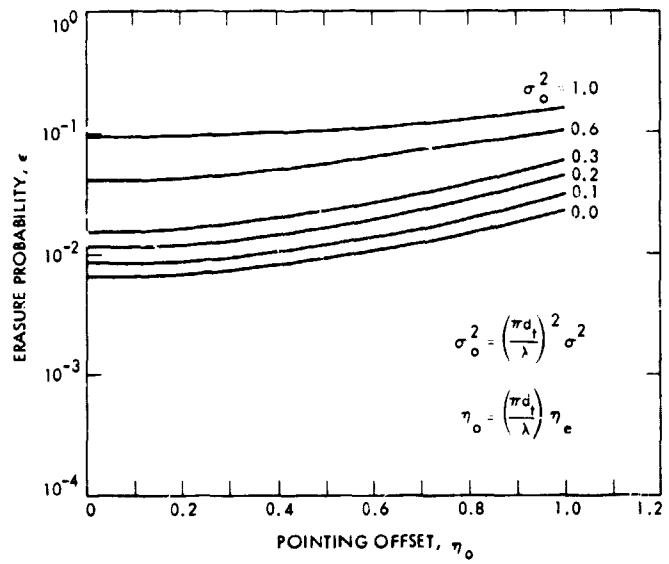

Figure 2-16c. Erasure Probability in the Presence of Random Pointing Errors: Average Signal Count = 5

SECTION 3

THE OPTICAL-RF COMMUNICATION INTERFACE

The use of cascaded optical RF communications links between deep space vehicles and Earth-based RF receivers by means of orbiting relay satellites presents some interesting communications interface problems. The interface is required to transform the received optical data into signal formats suitable for transmission over the RF relay channel (see Fig. 1-1). The interface problem is basically one of matching the link parameters to achieve the desired overall performance, while avoiding the overdesign of either link.

Consider the model of the data return link between the spacecraft, the relay receiver, and the ground station shown in Fig. 3-1. We assume that the RF link can maintain a data rate of R_{RF} bits/second, using an RF bandwidth of B_{RF} Hz, with a prescribed bit error probability of PE_{RF}. The optical signal generates a shot noise process at the output of the photodetector. The photodetector gain is assumed to be sufficiently great, and the gain variance sufficiently small, to allow the application of photon counting techniques to the shot noise process. If the received optical pulses are τ seconds in duration, and the shot noise process is passed through a time invariant τ-second integrator, the single-sided bandwidth of the resulting waveform is approximately $B_o = 1/\tau$ Hz. The filtered shot noise waveform will be denoted by the time function $x(t)$. Note that if the inverse of the detector bandwidth is much less than the integration time, then the waveform $x(t)$ represents the total number of counts occurring over the past τ seconds, for all t. Hence, the filtered waveform may be sampled at synchronous τ second intervals to obtain the required pulse counts.

We distinguish between two fundamentally different interface alternatives. The relay receiver can either

(1) Decode the optical data at the relay, and retransmit the decoded data over the RF channel,

or

(2) Transmit the waveform $x(t)$ directly over the RF link, leaving the decoding operation for the ground station.

In the following sections we examine each of these interface alternatives in terms of practical link constraints.

3.1 SYSTEM A (DECODE AND RETRANSMIT)

This system decodes the photodetector output directly at the relay, and modulates the decoded bit stream onto a suitable RF carrier for transmission to the ground station. Note that accurate temporal synchronization must be established at the relay receiver in order to decode the optical signal. For this system, the optical data rate can be matched directly to the RF data rate:

$$R_o = R_{RF} \tag{3-1}$$

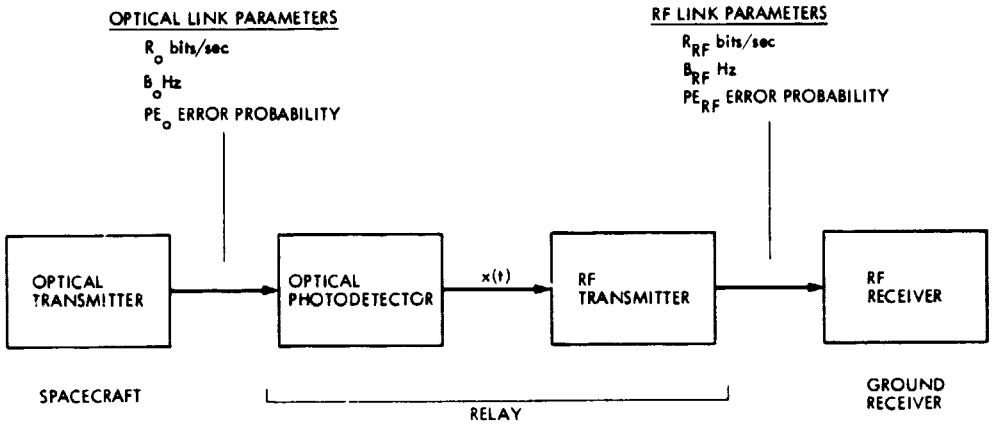

Figure 3-1. Block Diagram of the Optical-RF Interface

The resulting bit error probability at the ground station now becomes that of a cascaded pair of binary channels. If the bit error probability of the optical channel is PE_o, and that of the RF channel is PE_{RF}, then independent errors on each channel yield the expression

$$\begin{aligned} PE &= (1 - PE_o)\ PE_{RF} + (1 - PE_{RF})\ PE_o \\ &= PE_{RF} + PE_o - 2PE_{RF}\ PE_o \end{aligned} \tag{3-2}$$

Thus the overall bit error probability is determined by the larger of the individual error probabilities for the two separate links. This implies that the optical and RF links should be "matched" in digital performance. That is, each error probability should be as low as possible, but there is no significant advantage in having one link considerably better than the other.

For the noiseless optical channel, the equivalent bit error probability (for M-ary PPM signals) can be expressed as

$$PE_o = \frac{1}{2}\left(\frac{M}{M-1}\right) PWE = \left(\frac{1}{2}\right) e^{-K_s} \tag{3-3}$$

If the RF link is modeled as a binary additive Gaussian noise channel, then for antipodal PSK the error probability of the RF receiver can be expressed as

$$PE_{RF} = \left(\frac{1}{2}\right) \operatorname{erfc}\left(\sqrt{\frac{E_b}{N_0}}\right) \leq \left(\frac{1}{2}\right) e^{-(E_b/N_0)} \tag{3-4}$$

where erfc(•) is the complementary error function and E_b/N_0 is the ratio of the bit energy E_b to the noise spectral level N_0. Hence, matching the performance of the two links requires

$$K_s \cong \frac{E_b}{N_0} \tag{3-5}$$

The two links should therefore be designed so that the average number of optical pulse counts K_s at the relay receiver is roughly equal to the ratio E_b/N_0 established by the RF receiver, while maintaining the desired error probability PE.

3.2 SYSTEM B (RELAY AND DECODE)

This system modulates the RF carrier directly with the filtered waveform x(t), and transmits it to the ground station for decoding. The advantage of this system is that temporal synchronization need not be established at the relay, since the timing information can be extracted from the demodulated RF waveform at the ground station. The required RF bandwidth B_{RF} for distortionless transmission of the filtered waveform depends on the modulation format chosen for the RF channel. In particular, amplitude modulation (AM) requires

$$B_{RF} = 2B_o \tag{3-6}$$

where B_o is roughly the single-sided bandwidth of x(t). For frequency modulation (FM) with modulation index β, the required RF bandwidth becomes

$$B_{RF} = 2(\beta + 1)\ B_o \tag{3-7}$$

For a given RF bandwidth, and M-ary PPM optical modulation, the maximum allowable optical data rate can be expressed as

$$(R_o)_{max} = \frac{\log_2 M}{M} \left(\frac{B_{RF}}{2}\right) \text{ for AM} \tag{3-8a}$$

and

$$(R_o)_{max} = \frac{\log_2 M}{M(\beta + 1)} \left(\frac{B_{RF}}{2}\right) \text{ for FM} \tag{3-8b}$$

The optical data rate is clearly dependent on the available RF bandwidth. Note that for AM and narrowband FM (corresponding to $(\beta << 1)$ the optical data rates are comparable, but the use of wideband FM ($\beta >> 1$) decreases the allowed optical data rate by a factor of $(\beta + 1)$, for a given RF bandwidth. On the other hand, the advantages of constant amplitude modulation tend to favor FM modulation formats over AM modulation. The relative advantages of wideband and narrowband FM with respect to power levels, bandwidth requirements, and decoder performance remain to be investigated in greater detail.

The possible use of more sophisticated modulation formats should also be explored. For example, the filtered shot noise waveform can be sampled, the sample values quantized and the resulting data transmitted over a digital RF link to the ground station for decoding. It is apparent that the optical-RF interface problem presents some interesting design alternatives that bear further investigation from both theoretical and practical points of view.

SECTION 4

CONCLUSIONS AND RECOMMENDATIONS

The possible use of optical data links for deep space communication via a geostationary optical relay receiver has been examined. This type of system appears to be a promising alternative to RF systems for future deep space missions. It was shown that data rates on the order of 10^7 bits/sec at a bit error rate of 5×10^{-3} could be achieved over a range of 10^{12} meters using 1 meter transmitting optics, 1 watt optical source and a relay receiver with a collecting aperture of 4.5 meters. This communication rate is approximately 100 times greater than the Voyager 2 capability at the same range and error rate. Alternatively, for an optical communications system designed to operate at the same rate as the Voyager 2 RF system, the transmitter aperture requirement could be reduced to 10 cm or the communication range extended to 10^{13} meters. The various optical system parameters (required prime power, communications rate, optics size, system cost, etc.) can clearly be traded off to obtain the most advantageous design for any particular deep space mission.

The development of efficient, high power optical sources capable of generating the narrow optical beams required for deep space communications remains a topic of current research. It is apparent from the link analysis of Section 1 that transmitted optical power levels on the order of 0.1 to 1 watt are required for high data rate deep space communications, if the use of unreasonably large optics is to be avoided.

The problems of acquiring, tracking, and pointing both the uplink beacon and the downlink beams require further detailed analysis. Preliminary results presented here indicate that beacon acquisition in the presence of optical clutter (such as the illuminated Earth or the Moon) can be improved by the use of beacon modulation techniques that tend to distinguish the desired source from the interfering clutter. The effects of optical clutter and uniform background sources on the performance of the tracking system, and the development of techniques to combat these effects, require further study. Techniques for computing point-ahead angles to the required accuracy for the complicated geometries inherent in deep space to relay links, and models to assess the effects of point-ahead errors on dynamic link performance, need to be developed. The possible use of auxiliary RF links to aid in optical pointing and timing has also been proposed. Further research is required to determine the role of auxiliary RF systems in optical deep space communications.

The development of advantageous modulation, encoding and decoding techniques should be continued, in order to improve link performance. However, preliminary results indicate that acceptable performance can be achieved even with relatively simple modulation schemes such as binary on-off keying and M-ary pulse position modulation. Any improvement over the performance of these elementary modulation formats by the use of more sophisticated encoding and decoding techniques can be interpreted directly in terms of relaxed requirements on transmitter power or optics size, or in terms of extending the useful range of the optical link.

Finally, the optical-RF interface presents some interesting, and as yet unresolved, design alternatives. As pointed out in Section 3, the relay receiver can either decode the optical data and retransmit it to the ground station over an appropriate RF link, or transmit the detected (but not decoded) optical signals directly to the ground station for final processing. Further work is required to determine the most desirable strategy. The resolution of this question will undoubtedly have a significant impact on the design of the optical relay receiver.

ACKNOWLEDGEMENT

The authors wish to thank Jeffrey Osman for generating some of the numerical results.

REFERENCES

1. Vilnrotter, V. A., and Gagliardi, R. M. "Optical-Communication Systems for Deep Space Applications," Publication 80-7, Jet Propulsion Laboratory, Pasadena, California, March 15, 1980.

2. Vilnrotter, V. A., "Spatial Acquisition of Optical Sources in the Presence of Intense Interference," in the TDA Progress Report 42-58, pp. 91-96, Jet Propulsion Laboratory, Pasadena, California, Aug. 15, 1980.

3. Vilnrotter, V. A., "The Effects of Pointing Errors on the Performance of Optical Communications Systems," in the TDA Progress Report 42-63, Jet Propulsion Laboratory, Pasadena, California, June 15, 1981.

4. McEliece, R. J. and Welch, L. R., "Coding for Optical Channels with Photon Counting," in the DSN Progress Report 42-52, Jet Propulsion Laboratory, Pasadena, California, Aug. 15, 1979.

5. Massey, J. L., "Capacity, Cutoff Rate and Coding for a Direct-Detection Optical Channel," in the TDA Progress Report 42-60, Jet Propulsion Laboratory, Pasadena, California, Dec. 15, 1980.

6. Gagliardi. R. M., and Karp, S., Optical Communications, J. Wiley and Son, 1976.

7. Gaglardi, R. M., and Sheikh, M., "Pointing Error Statistics in Optical Beam Tracking," IEEE Trans. on Aerospace and Electronics Systems, Vol. AES 26, No. 10, Sept. 1980.

8. Ross, M., et al., "Space Orbital Communications with the N_d-Y_{ag} Laser," Proc. of the IEEE, Vol. 66, No. 3, pp. 319-344, March 1978.

9. Born, M., and Wolf, E., Principles of Optics, Pergamon Press, New York, 1975.

10. Gagliardi, R. M., Introduction to Communication Engineering, Wiley, 1978.

11. Sergeyevsky, A.B., Mission Design Data for Venus, Mars, and Jupiter through 1990, Technical Memorandum 33-736, Vol. III, Jet Propulsion Laboratory, Pasadena, California, Sept. 1, 1975.

APPENDIX A

OPTICAL BEACON TRACKING

A.1 INTRODUCTION

Optical beacon tracking systems are often employed in optical communication links. The purpose of the tracking system is to keep the incoming beam properly centered in the detector plane in spite of beam wander and/or relative motion between the transmitter and receiver. Errors in tracking translate directly to beam power losses in reception, and to pointing losses in transmission. Hence the design of an optical tracker becomes an integral part of the overall communication link construction. In this appendix we show that the design of optical beacon trackers parallels the design of the more familiar phase or pulse tracking system, and procedures and design equations for the two systems are significantly similar.

Beacon tracking involves generation of simultaneous error voltages corresponding to the changes in azimuth and elevation angles of the arriving beacon. These error voltages are generated by an optical sensor and are proportional to the offset alignment errors between receiver and beam arrival that may occur. Error voltages are then used to control both azimuth and elevation alignments and two separate tracking loops are required. This means that beam tracking is inherently a two-loop, or two-dimensional, tracking operation, and should therefore be investigated via tracking error vectors, rather than error scalars as in phase theory.

A.2 GENERAL TRACKER MODEL

A general beam tracking system is shown in Fig. A-1. The position error sensor produces both azimuth and elevation tracking error voltages. These error voltages are in turn used to generate alignment control signals. This is accomplished by control loop dynamics, generally with separate servo-loops for control of azimuth and elevation coordinates, respectively. The loop control functions are typically low pass filters which smooth out the error signal for proper control. The filtered control signals in azimuth and elevation are then used to step servo motors or tilt gimbals so as to properly realign the optical system.

Denote the azimuth and elevation angles of the arriving beam as (θ_z, θ_ℓ) and the azimuth and elevation angles of the normal vector to the receiving area as (ϕ_z, ϕ_ℓ). The instantaneous angular pointing errors are therefore

$$\psi_z = \theta_z - \phi_z \text{ rad} \tag{A-1a}$$

$$\psi_\ell = \theta_\ell - \phi_\ell \text{ rad} \tag{A-1b}$$

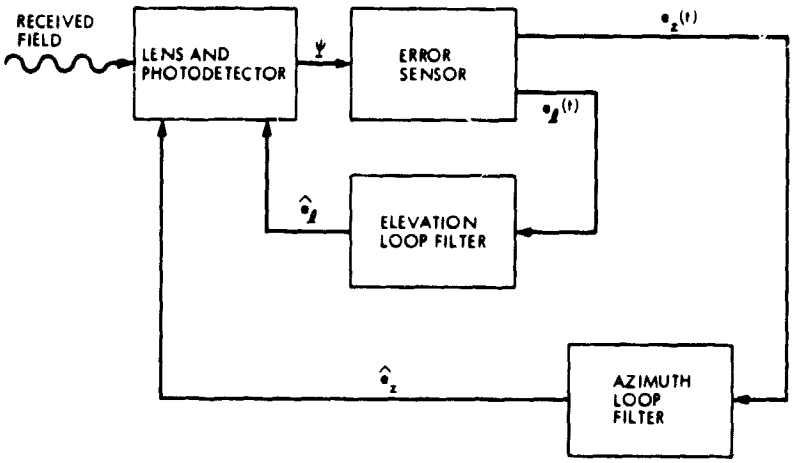

Figure A-1. Tracking System Block Diagram

where the time dependence has been deleted (Fig. A-2). Let $e_z(t)$ and $e_\ell(t)$ be the voltages generated by the position error sensor for control of azimuth and elevation angles, respectively. Let $\hat{e}_z(t)$ and $\hat{e}_\ell(t)$ be the filtered versions of control voltages due to the loop control filters. Hence we write

$$\hat{e}_z(t) = \int_0^t e_z(\rho)\, f_z(t - \rho)\, d\rho \tag{A-2a}$$

$$\hat{e}_\ell(t) = \int_0^t e_\ell(\rho)\, f_\ell(t - \rho)\, d\rho \tag{A-2b}$$

where $f_z(t)$ and $f_\ell(t)$ are the loop filter impulse responses of each loop.

It should be noted that the error signals $e_z(t)$ and $e_\ell(t)$ are both functions of the error vector $\underline{\psi} = (\psi_z, \psi_\ell)$ in (A-1). Since $\underline{\psi}(t)$ will evolve as random process, it is convenient to write $\hat{e}(t)$ in terms of its conditional mean,[4]

$$e(t) = E\left[\hat{e}(t) \,|\, \underline{\psi}(t)\right] + n(t) \tag{A-3}$$

where

$$n(t) \triangleq \hat{e}(t) - E\left[\hat{e}(t) \,|\, \underline{\psi}(t)\right] \tag{A-4}$$

[4] We drop the azimuth and elevation subscript since the same type of equation holds in both cases.

Here n(t) represents an effective detector noise added to the mean error signal. Any additional circuit noise can be directly incorporated into n(t). The positioning gimbals or servos respond to the error voltage by producing proportional angular velocities. Hence angular position varies as the integral of the filtered control signal. In addition, there may be unintentional position variations due to random structure flexures or gimbal variations, which appear as an added random position error $\phi_n(t)$ superimposed on the receiver pointing. Hence, we can write

$$\phi(t) = G_g \int_0^t \hat{e}(x)\, dx + \phi_n(t) \tag{A-5}$$

where G_g is a gimbaling proportionality gain in rad/volt. Combining (A-1) - (A-5) yields the pair of system equations

$$\frac{d\Psi_z}{dt} = \frac{d\theta_z}{dt} - G_g F_z \left\{ E\left[e_z(t) \,|\, \underline{\psi}(t) \right] + n_z(t) \right\} - \frac{d\phi_{nz}}{dt} \tag{A-6a}$$

$$\frac{d\Psi_\ell}{dt} = \frac{d\theta_\ell}{dt} - G_g F_\ell \left\{ E\left[e_\ell(t) \,|\, \underline{\psi}(t) \right] + n_\ell(t) \right\} - \frac{d\phi_{n\ell}}{dt} \tag{A-6b}$$

where F_z and F_ℓ are the convolution operators in (A-2). Here $d\theta_z/dt$ and $d\theta_\ell/dt$ represent the movement of the line-of-sight vector and appear as forcing functions. Equation (A-6) represents a pair of coupled (through the error function) set of stochastic equations that describe the joint beam tracking operation. The specific form of the differential equations is dependent upon the nature of the error voltages (which in turn are dependent upon the properties of the error sensor) and the type of loop filtering.

A.3 CW BEACON TRACKING WITH A QUADRANT DETECTOR

The most common type of optical sensor used in beam tracking systems is the quadrant detector (Fig. A-2). When the received optical field arrives normal to the receiver lens, it is focused on the center of the quadrant detector, and the resulting intensity pattern in the detector plane is centered at the origin. Offsets in arrival angles cause an imbalance in individual detector energies, which in turn are used to generate correcting voltages.

Let $m_i(t)$ denote the output current (due to signal, background noise, dark current) produced by the i^{th} quadrant detector. The azimuth and elevation error signals are given by:

$$\hat{e}_z(t) = \left[m_1(t) + m_2(t) \right] - \left[m_3(t) + m_4(t) \right] \tag{A-7a}$$

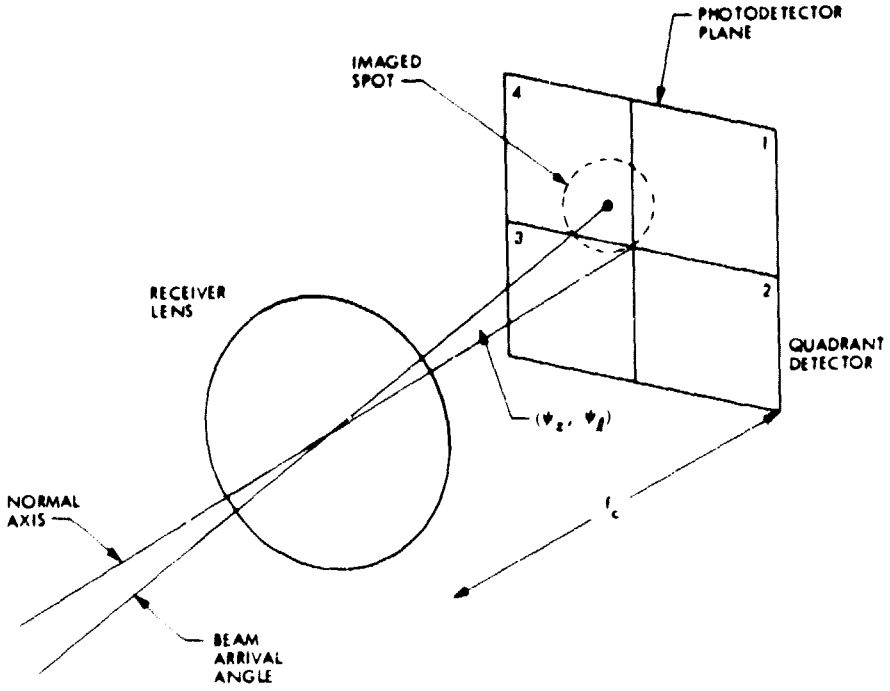

Figure A-2. Offset Images with Quadrant Photodetectors

$$\hat{e}_{\ell}(t) = \left[m_1(t) + m_4(t)\right] - \left[m_2(t) + m_3(t)\right] \qquad \text{(A-7b)}$$

Here $m_i(t)$ is a wideband, conditionally Poisson shot noise process with average intensity

$$\lambda_i(t) = G_d e\left(\frac{\eta_d}{h\nu}\right) \int_{A_i} I(\underline{r},t)\, d\underline{r} \; ; \quad i=1,2,3,4 \qquad \text{(A-8)}$$

where G_d is the mean detector gain, $I(\underline{r},t)$ denotes the spatial distribution of the optical field intensity in the receiver focal plane, A_i is the detecting area of the i^{th} detector, $\eta_d/h\nu$ is the detector efficiency divided by the energy of a photon, and e is the electron charge. We assume any individual detector dark current is included in $I(\underline{r},t)$.

We consider the important case when the received optical field is a monochromatic plane wave (CW beacon). In this case, if the beacon is pointed at the receiver lens, the source imaged in the detector plane is the Airy pattern of the receiver. When the incoming source field arrives normal to the receiver lens, the Airy pattern is centered at the origin of the quadrant detector and, on the average, the azimuth and elevation errors are zero (energy is equally

distributed on all four detectors). However, when the incoming field is offset by (Ψ_z, Ψ_ℓ) in azimuth and elevation respectively, the center of the Airy disk is shifted by $\Psi_z f_c$, $\Psi_\ell f_c$ in azimuth and elevation, where f_c is the receiver lens focal length (Fig. A-2).

A.3.1 Detector Error Characteristics

Under offset conditions, the mean error in (A-3) becomes, using (A-7) and (A-8),

$$E(\hat{e}_z|\underline{\Psi}) = E\left[m_1 + m_2 - m_3 - m_4 \,|\, \underline{\psi}\right]$$

$$= G_d e \frac{\eta d}{h\nu} \left\{ \int_{A_1} \left[I_s(\underline{r}) + I_n \right] d\underline{r} + \int_{A_2} \left[I_s(\underline{r}) + I_n \right] d\underline{r} \right. \tag{A-9}$$

$$\left. - \int_{A_3} \left[I_s(\underline{r}) + I_n \right] d\underline{r} - \int_{A_4} \left[I_s(\underline{r}) + I_n \right] d\underline{r} \right\}$$

where $I_s(\underline{r})$ is the offset Airy pattern and I_n is a uniformly distributed background intensity, which may be present in some applications.

If all detectors in the quadrant are balanced (i.e., have equal gain, areas, efficiencies, and dark currents), the terms involving I_n cancel. The remaining terms involving $I_s(\underline{r})$ will then correspond to the difference of the integrated offset Airy patterns over pairs of detector areas. It can then be easily seen that as long as the Airy pattern remains entirely on the detectors, the resulting $E(\hat{e}_z|\underline{\Psi})$ depends only on Ψ_z, and similarly, $E(\hat{e}_\ell|\underline{\Psi})$ depends only on Ψ_ℓ. Hence, a large quadrant detector "uncouples" the tracking operation by generating separate mean error signals in azimuth and elevation. The point source tracking in azimuth and elevation can therefore be treated as independent operations, and separate scalar analyses can be performed on each. If the quadrant detector is not balanced, an offset bias term must be added to (A-9).

The offset Airy pattern is conveniently written in terms of the centered Airy pattern as $I_s(x,y) = I_s^c(x - \Psi_z f_c, y - \Psi_\ell f_c)$. The centered Airy pattern takes the form (see Eqs. (2-15), (2-17))

$$I_s^c(x,y) = P_s \frac{\pi d^2}{\lambda^2 f_c^2} \left[\frac{J_1^2\left[u(x,y)\right]}{u^2(x,y)} \right] \tag{A-10}$$

where

$$u(x,y) = \frac{\pi d_t}{\lambda f_c} \sqrt{x^2 + y^2} \tag{A-11}$$

and P_s is the integrated intensity

$$P_s = \int I_s(\underline{r})\, d\underline{r} \simeq \sum_{i=1}^{4} \int_{A_i} I_s(\underline{r})\, d\underline{r} \tag{A-12}$$

The approximate equality in (A-12) is valid to the extent that most of the Airy pattern remains on the detector.

It is convenient to reference the integrated intensity difference in (A-9) to the integrated intensity P_s. Also define

$$n_s = \frac{\eta_d}{h\nu} P_s \tag{A-13}$$

as the average total photon count rate due to the arriving signal beam over all four quadrants. Then the mean error expression (A-9) can be written as

$$E(\hat{e}_z | \Psi_z) = n_s G_d e S(\Psi_z) \tag{A-14}$$

where

$$S(\Psi_z) = \frac{1}{P_s}\left[\int_{A_1} I_s(\underline{r})\, d\underline{r} + \int_{A_2} I_s(\underline{r})\, d\underline{r} - \int_{A_3} I_s(\underline{r})\, d\underline{r} - \int_{A_4} I_s(\underline{r})\, d\underline{r} \right] \tag{A-15}$$

A similar expression describes the mean elevation error,

$$E(\hat{e}_\ell | \Psi_\ell) = n_s\, G_d e\, S(\Psi_\ell) \tag{A-16}$$

The functions $S(\Psi)$ appearing in (A-14) and (A-16) are equal by virtue of the symmetry of the Airy pattern.

The function $S(\Psi)$ represents the error detector characteristic of the azimuth and elevation tracking loop (often called the loop S-curve). It satisfies the inequality $|S(\Psi)| \leq 1$. For the geometry of an infinite quadrant detector and an Airy pattern offset of $(\Psi_z f_c, \Psi_\ell f_c)$ from the detector center, the error characteristic is evaluated as

$$S(\Psi_z) = \frac{1}{P_s} \int_{-\infty}^{\infty} dy \left[\int_0^{\infty} dx\ I_s^c\ (x - \Psi_z f_c,\ y - \Psi_\ell f_c) - \int_{-\infty}^{0} dx\ I_s^c(x - \Psi_z f_c,\ y - \Psi_\ell f_c) \right]$$

$$= \frac{1}{P_s} \int_{-\infty}^{\infty} dy \left[\int_{-\Psi_z f_c}^{\infty} dx\ I_s^c\ (x,y) - \int_{-\infty}^{-\Psi_z f_c} dx\ I_s^c\ (x,y) \right]$$

$$= \frac{2}{P_s} \int_{-\infty}^{\infty} dy \int_0^{\Psi_z f_c} dx\ I_s^c(x,y) \qquad \text{(A-17)}$$

The last equality follows from the symmetry of the centered Airy pattern. When the explicit form (A-10) of the Airy pattern is substituted into (A-17) the double integral can be reduced to a single integral in two equivalent forms

$$S(\Psi) = 1 - \int_0^{2\pi} d\theta \left[J_0^2 \left(\Psi \frac{\pi d}{\lambda} \csc\ \theta \right) + J_1^2 \left(\Psi \frac{\pi d}{\lambda} \csc\ \theta \right) \right]$$

$$= \frac{4}{\pi} \int_0^{\infty} du\ \frac{J_1^2(u)}{u} \sin^{-1} \left[\min \left(1,\ \Psi \frac{\pi d}{\lambda u} \right) \right] \qquad \text{(A-18)}$$

This error characteristic is sketched in Fig. A-3.

The derivation of (A-18) assumes that the Airy pattern is always encompassed by the quadrant detectors. A saturation effect occurs as the error slides the Airy pattern off the quadrant crosshairs. If the error continues to increase, the Airy pattern eventually slides off the detecting surface, and $S(\Psi)$ decreases to zero. This means that the angle error in azimuth or elevation is outside the conical field of view of the receiver lensing system. Note that the loop error function is nonlinear but has no "false zeros." Therefore, the tracking system will either "pull-in" (drive to zero) or operate outside the field of view (lose lock).

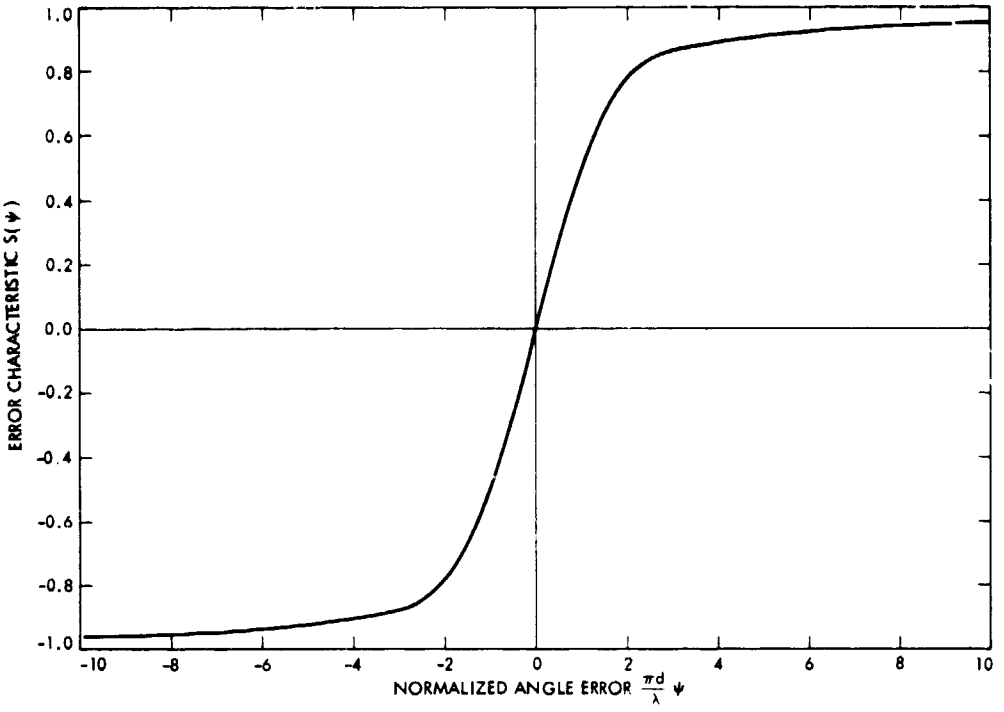

Figure A-3. Tracking Loop Error Detector Characteristic

A.3.2 Tracking Loop Error Analysis

When (A-14) and (A-16) are used in (A-6) with the systems uncoupled, each tracking equation reduces to the form

$$\frac{d\Psi}{dt} = \frac{d\theta}{dt} - G_g F \left\{ n_s G_d e\, S(\Psi) + n(t) \right\} - \frac{d\phi_n}{dt} \qquad \text{(A-19)}$$

Equation (A-19) is reminiscent of the basic phase lock system equation, and corresponds to the tracking loop model in Fig. A-4. The loop filter function F(s) is the Laplace operator corresponding to the operator $F\{\cdot\}$ in (A-6), and is the transform of f(t) in (A-2). Hence the system tracks in azimuth and elevation through a pair of loops, each modeled by Fig. A-4, operating disjointly and in parallel. Note that the error variable in the loop corresponds to angular error in pointing instead of the usual phase variable.

Since the loop model is similar to that of a phase tracking system, much of the tracking analysis carries over directly. If we assume small tracking errors, we can linearize the detector error characteristic $S(\Psi)$ around $\Psi = 0$,

$$S(\Psi) \simeq S'(0)\,\Psi$$

$$= \frac{16}{3\pi} \frac{d}{\lambda} \Psi \qquad \text{(A-20)}$$

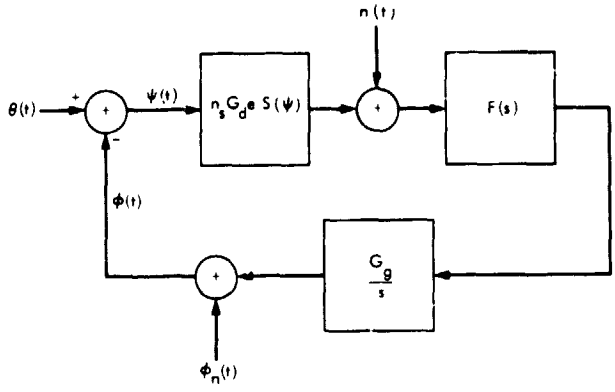

Figure A-4. Equivalent Tracking Error Block Diagram

where λ is the optical beam wavelength and d is the receiver lens diameter. Fig. A-4 reduces to a linear tracker, with the loop gain function

$$H(s) = \frac{G_L F(s)}{s + G_L F(s)} \tag{A-21}$$

where

$$G_L = \frac{16}{3\pi} n_s\, G_d e\, G_g \frac{d}{\lambda} \tag{A-22}$$

is the effective loop gain.

The loop noise n(t) is the combined photodetector shot noise and circuit thermal noise. For wideband photodetectors, the shot noise has spectral level

$$S_{sn}(\omega) = (G_d e)^2 \left(n_s + 4n_b\right) \tag{A-23}$$

where n_s is given in (A-13) and

$$n_b = \frac{\eta_d}{h\nu} I_n A_i \tag{A-24}$$

is the individual detector background count rate. To the shot noise level must be added the circuit noise spectral level N_{oc}, dependent on the receiver noise temperature. The total noise spectrum is thus

$$S_n(\omega) = S_{sn}(\omega) + N_{oc}$$
$$= (G_d e)^2 (n_s + 4n_b) + N_{oc} \tag{A-25}$$

The mean square pointing error in azimuth or elevation for the loop in Fig. A-4 is then

$$\sigma_\psi^2 = \frac{2S_n(0)\ B_L}{\left(\frac{G_L}{G_g}\right)^2} \tag{A-26}$$

where the loop bandwidth B_L is as usually defined,

$$B_L = \frac{1}{2\pi} \int_0^\infty |H(\omega)|^2\ d\omega \tag{A-27}$$

Thus (A-26) can be rewritten as

$$\sigma_\psi^2 = \frac{\left(\frac{\lambda}{d}\right)^2}{\gamma} \tag{A-28}$$

where

$$\gamma = \left(\frac{16n_s}{3\pi B_L}\right) \left[\frac{n_s}{n_s + 4n_b + \left(\frac{N_{oc}}{G_d^2 e^2}\right)} \right] \tag{A-29}$$

The angular tracking error variance due to receiver noise is therefore inversely related to the parameter γ, which plays the role of a loop signal-to-noise ratio, much like in a phase tracking system. Recalling that the diffraction limited beam angle is approximately

$$\theta_{dL} \simeq \frac{\lambda}{d} \tag{A-30}$$

we see that the rms tracking error in (A-28) is equivalently

$$\sigma_{\psi} = \frac{\theta_{dL}}{\sqrt{\gamma}} \tag{A-31}$$

Thus the receiver tracker can be expected to track to within a fraction of the diffraction limited beamwidth of its receiving lens, for $\gamma \gg 1$.

Note from (A-29) that the parameter γ can also be interpreted as

$$\gamma = \left(\frac{16\ n_s}{3\pi B_L}\right) S_L \tag{A-32}$$

where S_L is the bracketed quantity in (A-29). Since $S_L \leq 1$, it appears as an effective "squaring loss" that degrades performance as the noise increases, much like that in phase lock squaring loops. Interestingly, we note that if the noise goes to zero, γ does not become infinite, but instead approaches the quantum limited value

$$\gamma \rightarrow \frac{16\ n_s}{3\pi B_L} \tag{A-33}$$

Since n_s is the signal beacon count rate, (A-33) corresponds to the number of beacon signal photoelectrons that will be produced in a $16/3\pi B_L$ time period. This therefore determines the ultimate limit in beam tracking.

Lastly, it should be remembered that both azimuth and elevation may simultaneously produce independent errors (under the uncoupled assumption). Thus the instantaneous total rms error in tracking is actually,

$$\psi_{rms} \triangleq \sqrt{E|\underline{\psi}|^2} = \sqrt{2\sigma_{\psi}^2} = \frac{1.4\,\theta_{dL}}{\sqrt{\gamma}} \tag{A-34}$$

The gimbal positioning noise can be handled by similar analyses. Let $S_g(\omega)$ be the spectrum of the spectral vibration of the gimbals (usually a 1/f type vibration at low frequencies). The pointing error spectrum due to the loop's attempt to correct this vibration is given by $S_g(\omega)\ |1 - H(\omega)|^2$. The resulting mean square positioning error due to gimbal noise is then

$$\sigma_g^2 = \frac{1}{2\pi} \int_{-\infty}^{\infty} S_g(\omega)\ |1 - H(\omega)|^2\ d\omega \qquad \text{(A-35)}$$

It is clear that the tracking loop bandwidth should be large enough to exceed the significant frequencies of the gimbal vibration. The mean squared error in (A-35) must be added directly to that in (A-28) to determine the total tracking error. Note that gimballing noise in pointing systems acts much the same as VCO noise in phase lock systems.

A.3.3 Clutter Effects

A common problem in beacon tracking is the presence of unwanted light sources, or clutter, in the tracking field of view. Such clutter appear as false targets, as opposed to the constant intensity sky background which uniformly illuminates the tracker detector. If significantly bright, the clutter can capture the tracker, and cause large errors in the tracking of the desired point source.

To account for these effects in the system model, we reexamine (A-9) with a clutter intensity added. The imaged field intensity at the receiver is then

$$I(\underline{r},t) = I_s(\underline{r},t) + I_c(\underline{r},t) + I_n, \qquad \text{(A-36)}$$

where $I_c(\underline{r}, t)$ is the spatially distributed intensity due to the clutter as it moves in time. Substituting into (A-9), assuming a balanced quadrant detector, then yields

$$E(\hat{e}(t)\,|\,\Psi_s) = n_s G_d e\ S(\Psi_s) + C(t) \qquad \text{(A-37)}$$

where

$$C(t) = G_d e \frac{\eta_d}{h\nu} \int_{\substack{\text{quad}\\ \text{diff}}} I_c(\underline{r},\ t)\ d\underline{r} \qquad \text{(A-38)}$$

and Ψ_s is the tracking angle error relative to the true source. In (A-38) the integral is over area differences, depending on whether azimuth or elevation is being tracked. The function C(t) is the mean voltage that the clutter adds to the quadrant detector output as it moves in the image plane of the receiver.

To interpret this equation, denote

$$n_c(t) = \frac{\eta_d}{h\nu} \sum_{i=1}^{4} \int_{A_i} I_c(\underline{r}, t)\, d\underline{r} \tag{A-39}$$

as the total photodetector count at the receiver due to clutter, and define

$$\Psi_c(t) = S^{-1}\left[\frac{C(t)}{G_d e\, n_c(t)}\right] \tag{A-40}$$

as the effective angle error the clutter would have if it were a point source with the same total power. This allows us to write (A-37) as due to a combined, single point source

$$E(\hat{e}(t)\,|\,\Psi_s) = G_d e\left[(n_s + n_c)\, S(\Psi_e)\right] \tag{A-41}$$

with total power $(n_s + n_c)$ and equivalent angle Ψ_e defined by

$$(n_s + n_c)\, S(\Psi_e) = n_s S(\Psi_s) + n_c S(\Psi_c) \tag{A-42}$$

or equivalently,

$$\Psi_e = S^{-1}\left[\left(\frac{n_s}{n_s + n_c}\right) S(\Psi_s) + \left(\frac{n_c}{n_s + n_c}\right) S(\Psi_c)\right] \tag{A-43}$$

Neglecting shot noise and thermal noise, the system differential equation then becomes

$$\frac{d\Psi_s}{dt} = \frac{d\theta}{dt} - G_g G_d e\; F\left[(n_s + n_c)\, S(\Psi_e)\right] \tag{A-44}$$

This shows that clutter enters the system equation by altering the mean tracking signal. Assuming no source motion ($d\theta/dt = 0$), stationary clutter (n_c, Ψ_c do not depend on time), and a first-order loop, (A-44) will have the steady-state solution

$$\frac{d\Psi_s}{dt} = 0$$

$$S(\Psi_e) = 0 \qquad \text{(A-45)}$$

The last condition requires

$$\frac{n_s}{n_s + n_c} S(\Psi_s) = - \frac{n_c}{n_s + n_c} S(\Psi_c) \qquad \text{(A-46)}$$

Thus, the tracker will settle to a pointing angle such that the pointing error to the true source (Ψ_s) and to the effective clutter point (Ψ_c) satisfies (A-46). This adjustment is made in both azimuth and elevation simultaneously. In particular, note that the tracker will not in general point to either the source or the clutter, but instead at an intermediate angle given by the effective centroid angle Ψ_e. If $n_s >> n_c$ (bright source, dim clutter) (A-46) implies that $\Psi_s \simeq 0$; i.e., the system tracks the source. If $n_c >> n_s$ (strong clutter), $\Psi_c \simeq 0$, and the loop tracks the clutter. Thus, bright clutter in the field of view can pull the tracker away from the true source and the amount of offset is dependent on the relative strengths of each. It is significant that the shape of the imaged clutter is not important, only its total power level n_c and equivalent angle Ψ_c. The possibility of clutter (stars, moon, planets, etc.) influencing an optical tracker may be a serious problem in deep space optical links.

APPENDIX B

EFFECTS OF SPACECRAFT/RELAY RELATIVE MOTIONS

B.1 RELATIVE VELOCITY COMPONENTS

The relative velocity V of the relay and the spacecraft can be conveniently broken into three components:

$$V = V_E + V_r - V_s \tag{B-1}$$

where

V_E = velocity of Earth relative to the Sun

V_r = velocity of relay relative to Earth

V_s = velocity of spacecraft relative to the Sun

As a function of time, the vector V_E consists of two sinusoidally varying components in the ecliptic plane, with nearly constant magnitude $|V_E|$ equal to Earth's orbital velocity:

$$|V_E| = 30 \text{ km/sec} \tag{B-2}$$

The vector V_r consists of two sinusoidally varying components in the (equatorial) plane of the relay's orbit, with magnitude $|V_r|$ equal to the speed of a geostationary satellite:

$$|V_r| = 3 \text{ km/sec} \tag{B-3}$$

The velocity V_s may likewise be broken down into Sun-orbiting and planet-orbiting components if the spacecraft is being captured by a planet during an encounter, or it may represent the cruise velocity of the spacecraft between encounters.

It is convenient to decompose the components of the relative velocity vector into radial and tangential motions (subscripts R, T, respectively) relative to the spacecraft-relay LOS. In terms of the angles defined in Fig. 2-3, the radial and tangential velocity components are given by

$$\begin{aligned}
(V_E)_R &= |V_E| \cos \omega_E t \cos \beta \\
(V_E)_T &= |V_E| (\sin \omega_E t, \cos \omega_E t \sin \beta) \\
(V_r)_R &= |V_r| \cos \omega_r t \cos \delta \\
(V_r)_T &= |V_r| (\sin \omega_r t, \cos \omega_r t \sin \delta)
\end{aligned} \tag{B-4}$$

where

$$\omega_E = \frac{2\pi}{365 \text{ days}} = 0.72 \times 10^{-3} \text{ rad/hr}$$

$$\omega_r = \frac{2\pi}{24 \text{ hr}} = 0.26 \text{ rad/hr} \qquad \text{(B-5)}$$

In these equations the time origin has been chosen independently for V_E and V_r since the effects due to each are discussed separately. An appropriate relative phase must be included in order to study the effects jointly. The axis orientation in the tangent plane has been chosen in a simple manner for convenience (one axis perpendicular to the relay-spacecraft LOS). Additional terms involving the time derivatives of β and δ should also be included in (B-4) but are ignored as causing second-order effects.

The acceleration vectors $\dot{V}_E = dV_E/dt$ and $\dot{V}_r = dV_r/dt$ are similarly calculated as

$$(\dot{V}_E)_R = - |V_E| \, \omega_E \sin \omega_E t \cos \beta$$

$$(\dot{V}_E)_T = |V_E| \, \omega_E \, (\cos \omega_E t, \; -\sin \omega_E t \sin \beta)$$

$$(\dot{V}_r)_R = - |V_r| \, \omega_r \sin \omega_r t \cos \delta \qquad \text{(B-6)}$$

$$(\dot{V}_r)_T = |V_r| \, \omega_r \, (\cos \omega_r t, \; -\sin \omega_r t \sin \delta)$$

The radial and tangential motions of the spacecraft may be calculated in a similar manner for the case when the spacecraft is captured by another planet. The magnitude of the Sun-orbiting component of V_s is roughly equal to $|V_E|(R_E/R_p)^{1/2}$ and its frequency is roughly $V_E(R_E/R_p)^{3/2}$, where R_E and R_p are, respectively, the orbit radii of Earth and the planet which has captured the spacecraft. For encounters with the outer planets ($R_p >> R_E$), these motions always contribute significantly less to the overall relative motion than does the Earth velocity vector V_E. The planet-orbiting component of V_s is critically dependent on the actual orbit chosen. Its contribution can be either more significant or less significant than the corresponding contribution from the Earth-orbiting motion of the relay.

Additional trajectory information is also needed for the case when the spacecraft is cruising between planets. For the remainder of the analysis here, only the contributions from V_E and V_r to the relative motion will be considered.

B.2 DOPPLER SHIFTS

The fractional Doppler shifts due to the velocity components V_E and V_r are

$$\left(\frac{\Delta f}{f}\right)_E = \frac{(V_E)_R}{c} = 10^{-4} \cos \omega_E t \cos \beta$$

$$\left(\frac{\Delta f}{f}\right)_r = \frac{(V_r)_R}{c} = 10^{-5} \cos \omega_r t \cos \delta \qquad \text{(B-7)}$$

Thus the largest Doppler shift occurs when the relay-spacecraft LOS is parallel to the ecliptic plane ($\beta = 0$). If the transmitted wavelength is 1 micron, the wavelength shift for this case varies sinusoidally between ±1 Å over a one-year period. Similarly, the largest Doppler shift due to V_r occurs when the relay-spacecraft LOS is parallel to the equatorial plane ($\delta = 0$), and for 1-micron radiation this shift varies between ±1/10 Å throughout a 1-day period.

The rates of change of the fractional Doppler shifts are in turn given by

$$\left(\frac{\dot{\Delta f}}{f}\right)_E = \frac{(\dot{V}_E)_R}{c} = (-0.72 \times 10^{-7}/\text{hr}) \sin \omega_E t \cos \beta$$

$$\left(\frac{\dot{\Delta f}}{f}\right)_r = \frac{(\dot{V}_r)_R}{c} = (-0.26 \times 10^{-5}/\text{hr}) \sin \omega_r t \cos \delta \qquad \text{(B-8)}$$

Thus the Doppler drift is generally much faster due to Earth-orbiting motion than to Sun-orbiting motion, but for 1-micron radiation the worst-case drift here is only 0.026 Å per hour.

B.3 POINT-AHEAD ANGLE VARIATIONS

The required point-ahead angle components due to V_E and V_r are approximately[4] given by

$$|\alpha_E| = \frac{2}{c} |(V_E)_T| = (200\ \mu\text{rad}) \sqrt{1 - \cos^2 \omega_E t \cos^2 \beta}$$

$$|\alpha_r| = \frac{2}{c} |(V_r)_T| = (20\ \mu\text{rad}) \sqrt{1 - \cos^2 \omega_r t \cos^2 \delta} \qquad \text{(B-9)}$$

[4]The expression for the point-ahead angles should actually use an average of the vector tangential velocities over the round trip light time rather than the instantaneous tangential velocities indicated.

The angle $|\alpha_E|$ varies between 200 μrad and 200 (sin β) μrad over the course of a year, and the angle $|\alpha_r|$ varies between 20 μrad and 20 (sin δ) μrad over the course of a day. Both of these point-ahead angle components are significantly larger than the narrow optical beamwidths considered most useful for deep space applications, requiring accurate computation of their instantaneous values.

The rates of change in the point-ahead direction components are given by

$$|\dot{\alpha}_E| = \frac{2}{c} |(\dot{V}_E)_T| = (0.14\ \mu\text{rad/hr}) \sqrt{1 - \sin^2 \omega_E t \cos^2 \beta}$$

$$|\dot{\alpha}_r| = \frac{2}{c} |(\dot{V}_r)_T| = (5.2\ \mu\text{rad/hr}) \sqrt{1 - \sin^2 \omega_r t \cos^2 \delta} \qquad \text{(B-10)}$$

Thus, for optical beamwidths around 1 to 10 μrad and relay to spacecraft distances of 10 AU or so, the point-ahead angle must be readjusted at intervals shorter than the round-trip light time.

We point out that the point-ahead direction is actually two-dimensional, and the rates of change given in (B-10) are the magnitudes of the angular changes of the point-ahead vectors, and not merely the changes in their magnitude.